Multi-scale Modelling of the Cellular and Molecular Mechanisms of Hyperpolarisation mediated Synaptic Plasticity in the Vestibular Nuclei

Yubin Xie

Supervisor: Melanie I. Stefan

Master of Science

CENTRE FOR INTEGRATIVE PHYSIOLOGY

EDINBURGH MEDICAL SCHOOL UNIVERSITY OF EDINBURGH

Content

Abbreviation

α-amino-3-hydroxy-5-methyl-4-isoxazolepropionic receptor	AMPAR
Calcium	Ca^{2+}
Calcium concentration	$[Ca^{2+}]$
Ca^{2+}/calmodulin-dependent protein kinase II	CaMKII
Gamma-aminobutyric acid receptor	GABAR
Long-term depression	LTD
Long-term potentiation	LTP
Low-voltage activated calcium channel	LVCC
High-voltage activated calcium channel	HVCC
Medial vestibular nucleus	MVN
N-methyl-D-aspartate receptors	NMDAR
Protein phosphatase 1	PP1
Systems biology markup language	SBML
Voltage-dependent calcium channel	VDCC
Vestibular-ocular reflex	VOR

Abstract

Synaptic plasticity is assumed to underlie various forms of learning and memory. The classical theory believes that high-frequency presynaptic stimulation will induce long-term potentiation and low-frequency presynaptic stimulation will induce long-term depression, which are two forms of synaptic plasticity. Recently, for the first time, postsynaptic hyperpolarisation gated bidirectional plasticity was demonstrated in vestibular nerve synapses in the vestibular nucleus. In this system, the inhibitory Purkinje cells in the cerebellum can regulate the strength of excitatory neurotransmission in the vestibular nucleus neurons that they project to. This new type of plasticity is fully compatible with the proposed mechanism underlying motor learning during adaptation of the vestibulo-ocular reflex and can enhance our understanding of other forms of motor learning. However, the mechanistic cellular and molecular mechanisms behind this novel form of plasticity remain unknown. Here, I present a multi-scale model of hyperpolarisation mediated synaptic plasticity. This combines an electrical model of medial vestibular nucleus type B neurons in the vestibulo-ocular reflex system and comprehensive biochemical model of signalling pathway that underlies synaptic plasticity. In my model, I uncovered a complex relationship between Ca^{2+} concentration and synaptic strength. Then I found that presynaptic stimulation paired with hyperpolarisation can induce large amount of Ca^{2+} influx through low-voltage activated calcium channels, resulting in potentiation, and presynaptic stimulation without hyperpolarisation induce small amount of Ca^{2+} influx, resulting in depression. My finding reveals the cellular and molecular mechanisms underlying this novel plasticity and deepens our mechanistic understanding of motor learning.

Lay Summary

Synapses are the biological junctions between cells in our brain through which they communicate with each other and with other cells. The ability of synapses to change strength in response to their previous activities, which is termed as synaptic plasticity, is thought to underlie learning and memory. Traditionally, two forms of synaptic plasticity were known: If a nerve cell is activated at high-frequency in response to a strong signal, then the strength of its active synapses is increased. If it is activated at low-frequency in response to weaker signals, the strength of its synapses decreases. Recently, a new form of synaptic plasticity was discovered. It depends on hyperpolarisation, a decrease of neuron membrane potential. This plasticity was found in a brain region called the medial vestibular nucleus, which is involved in motor control. This new form of plasticity is fully compatible with the proposed mechanism underlying motor learning during adaptation of the vestibulo-ocular reflex. Understanding how this new form of synaptic plasticity works, will enhance our understanding of other forms of behavioural learning.

Here, I used computer software to simulate the electrical and chemical properties of medial vestibular nucleus neurons, and investigated the mechanisms of hyperpolarisation-dependent synaptic plasticity. I found that the decrease of electrical potential together with synaptic activity can adjust the synaptic strength, consistent with their role in motor learning. My findings reveal the mechanisms underlying this novel form of plasticity during motor learning and provide a more mechanistic understanding of how we adjust and optimise our movement.

1 Introduction

Animals not only behave differentially in specific environments but also can respond differently in the same situation over time. Such phenomena are macroscopic reflections of response specificity of neurons and involve memory storage and information processing. Fundamentally, this response property is achieved through the plasticity of synapses, which is therefore regarded as the basis of learning and memory. Thus, knowing the cellular and molecular mechanisms of synaptic plasticity: what temporal and spatial patterns of presynaptic neuronal activities trigger the plasticity, what molecular processes underlie such plasticity, and how the changes of synaptic strength consequently influence the behaviour, will deepen the understanding of how our brain stores information and forms memories, and consequently optimises our behaviour.

1.1 Synaptic plasticity

Synaptic plasticity is the ability of synapses between two neurons to change their strength (Hughes 1958). There are two forms of long-term plasticity (also called bidirectional plasticity): long-tern potentiation (LTP), a persistent strengthening of synapses, first discovered by Bliss and Lomo (1973), and long-term depression (LTD), a persistent weakening of synapses, first demonstrated by Lynch et al. (1977). Long-term plasticity allows the brain to adjust behaviour according to previous experience and therefore it is commonly assumed to be the neural mechanisms underlying various forms of information storage and processing (Hebb 1949; Eccles 1964; Alkon & Nelson 1990). Thus the study of this bidirectional plasticity is fundamental to understanding the neural basis and molecular mechanisms of learning and memory.

1.1.1 Molecular Mechanisms of Synaptic Plasticity

The specific patterns of cellular and synaptic activity that trigger bidirectional plasticity vary across brain regions and cell types (Citri & Malenka 2008). Generally, the induction of LTP and LTD at most glutamatergic synapses involves release of glutamate, postsynaptic depolarization (Debanne 1996) and influx of Ca^{2+} (Bear & Malenka 1994). The presynaptic glutamate release actives N-methyl-D-aspartate receptors (NMDARs), metabotropic glutamate receptors (mGluRs), and α-amino-3-hydroxy-5-methyl-4-isoxazolepropionic acid receptors (AMPARs). Postsynaptic depolarization, induced by activation of AMPARs, modulates VDCCs and activates NMDARs. Consequently, mGluRs, NMDARs and VDCCs together lead to an increase of intracellular Ca^{2+} concentration (Figure 1a) (Perkel et al. 1993), (Bear & Kirkwood 1993). And then, the increase of Ca^{2+} triggers the signalling

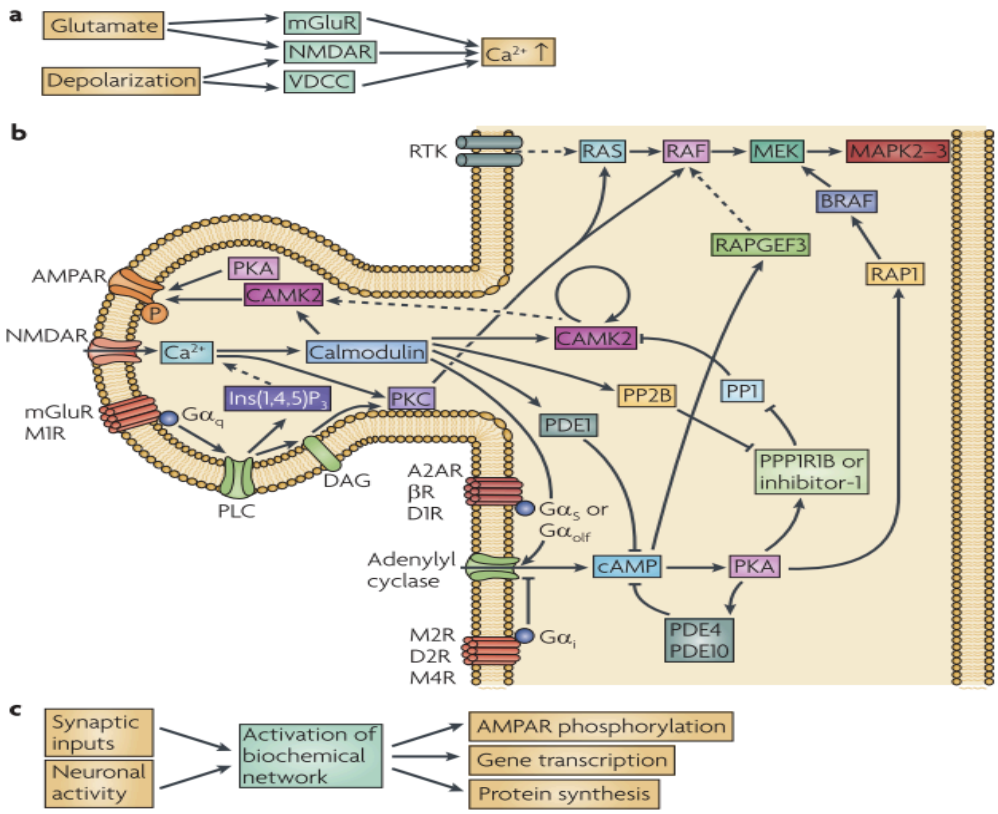

Figure 1 | **Signalling pathway of synaptic plasticity. a** | Presynaptic release of glutamate leads to the activation of mGluRs and NMDARs. Depolarization of postsynaptic neuron leads to the activation of NMDARs and VDCCs. Then the activation of mGluRs, NMDARs and VDCCs leads to Ca^{2+} influx into the postsynaptic cell. **b** | Signalling pathway implicated in synaptic plasticity (only the known pathways are illustrated and the pathways involved vary from neurons). The Ca^{2+} binds to calmodulin and the complex then binds to CaMKII or protein phosphatase 2B (PP2B/calcineurin). CaMKII is activated by autophosphorylation and can phosphorylate the AMPAR and contribute to LTP. PP2B inhibits inhibitor-1 or protein phosphatase 1 regulatory subunit 1B (PPP1R1), which inhibits Protein Phosphatase 1 (PP1), and eventually contributes to LTD. Adenylyl cyclase can produces the cyclic AMP and then activates protein kinase A (PKA), which phosphorylates the AMPAR and leads to LTP. Coupling the stimulatory G protein (GS) or olfactory G protein (G_{olf}) to β-adrenergic receptors (βRs), dopamine D1 receptors (D1Rs) and the adenosine type 2A receptor (A2AR) can activate adenylyl cyclase. While adenylyl cyclase can be inhibited by other muscarinic acetylcholine receptors (M2R&M4R) and dopamine D2 receptors (D2Rs). Phospholipase C (PLC) can be coupled to some muscarinic acetylcholine receptors (M1R) and mGluRs, which produce diacylglycerol (DAG). PKC can be activated by Ca^{2+} and DAG. The same as RAP guanine nucleotide exchange factor 3 (RAPGEF3), PKC, Ca2+ and PKA can indirectly activate MAPK2–3 (mitogen-activated protein kinase 2–3), which is involved in transcription and translation. **c** | the neuronal activity and synaptic inputs lead to AMPAR phosphorylation, gene transcription and protein synthesis by biochemical network (Kotaleski & Blackwell 2010).

pathways underlying plasticity (Figure 1b) and leads to changes in phosphorylation ratio of AMPAR, related gene transcription and protein synthesis (Figure 1c).

This type of synaptic plasticity is activity dependent. The timing and magnitude of Ca^{2+} elevations determine the induction of either potentiation or depression. The widely accepted theory about cellular mechanisms underlying plasticity describes plasticity as stimulation frequency dependent: High-frequency presynaptic stimulation causes fast and large Ca^{2+} influx. As a result, it will activate Ca^{2+}/calmodulin-dependent protein kinase II (CaMKII) pathways, which are required by for LTP (McGlade-McCulloh et al. 1993; Lledo et al. 1995). In contrast, a moderate increase of Ca^{2+} concentration, induced by low-frequency stimulation, activates the calcineurin pathway, leading to LTD (Mulkey et al. 1994).

Recently, hyperpolarisation mediated synaptic plasticity, in addition to classical activity-dependent plasticity, was demonstrated as being an important mechanism underlying cerebellum-dependent motor learning (Rothman et al. 2009; McElvain et al. 2010). In this relatively novel scenario, the activity of an inhibitory synapse can regulate the strength of neighbouring excitatory synapses by inducing LTP or LTD. Hyperpolarisation mediated LTP and LTD allow the inhibitory Purkinje cells in the cerebellum to regulate the strength of excitatory neurotransmission in the postsynaptic neurons that they project to, and therefore are significant in motor learning. The vestibulo-ocular reflex discussed below, as a typical example of cerebellum-dependent motor learning, is a perfect model to investigate this new plasticity.

1.2 The Vestibulo-Ocular Reflex

During our head movement, the vestibulo-ocular reflex (VOR) stabilises images on the retina by generating eye movement. To maintain such stable gaze on the objects of interest, the VOR triggers a quick (in less than 10ms Aw et al. 1996) and precise eye movement in the opposite direction of head movement in both rotational and translational aspects (Crawford & Vilis 1991; Angelaki 2004). This reflex prevents the image of object on the retina from slipping, and consequently increases visual acuity.

1.2.1 Plasticity in the Vestibulo-Ocular Reflex

Simple and well-characterised operation and neural circuitry, and more importantly, experience-dependent plasticity make the VOR well suited to study how activity-dependent synaptic plasticity drives motor learning.

The adaption of the VOR happens when the movement of the eyes cannot perfectly compensate for the movement of the head, and is reflected in the changes of the VOR gain, defined as the change in the eye angle divided by the change in the head angle (Wikipedia.org 2016). The VOR gain is constantly adjusted to ensure that the eye movement precisely compensates the head movement in the opposite direction (Miles & Lisberger 1981) (Figure 2A). Take Figure 2B1 as an example. When the strength of eye muscles is weakened, then the generated eye movement is less than the head movement. As a result, the image of the object slips on the retina. Consequently, resulting error signal of undercompensation will be generated in the accessory optic system in cerebellum and will lead to adaptive plasticity, which increases the firing rate output of the MVN neurons. Thus, the head movement is correctly compensated by the eye movement again. The neural basis of this VOR gain adaptation has been extensively investigated, and the site where the plasticity of the VOR gain is regulated has been of great interest (Medina 2010).

1.2.2 Mechanisms of Plasticity in the Vestibulo-Ocular Reflex

The Marr-Albus hypothesis positions inhibitory Purkinje cells in the cerebellar cortex as the site of the neural plasticity in the VOR gain adaptation (Marr 1969; Albus 1971; Ito 2002). In their pioneering theory, the error signals of retinal slip cause synaptic changes in the strength of the synaptic input into the Purkinje cells and modify their firing rate to recalibrate the reflex: increasing firing rate for overcompensation and decreasing firing rate for undercompensation. The experimental discovery of cerebellar LTD and LTP in Purkinje cells (Ito 2002), which is caused by retinal slip, strongly supports this hypothesis.

However, with plasticity residing only in the cerebellar cortex, the frequencies over which the VOR gain can be accurately calibrated are limited to about 2.5 Hz (Porrill & Dean 2007). This is because in reality the transmission of the retinal slip signals to the cerebellar cortex and Purkinje cells introduces a delay of around 100 ms (Stone & Lisberger 1990; Raymond & Lisberger 1998), limiting the frequencies over which the corrective calibration can operate. Instead of 2.5 Hz, the VOR can accurately calibrated at frequencies up to 25 Hz, which raises the question of how VOR gain calibration works for the frequencies higher than 2.5 Hz (Porrill & Dean 2007).

In 1981, Miles & Lisberger proposed that synapses of vestibular nerve onto the medial vestibular nucleus (MVN) neurons in brainstem could be an additional candidate site for adaption and hyperpolarisation as the possible mechanism of this plasticity. To be specific,

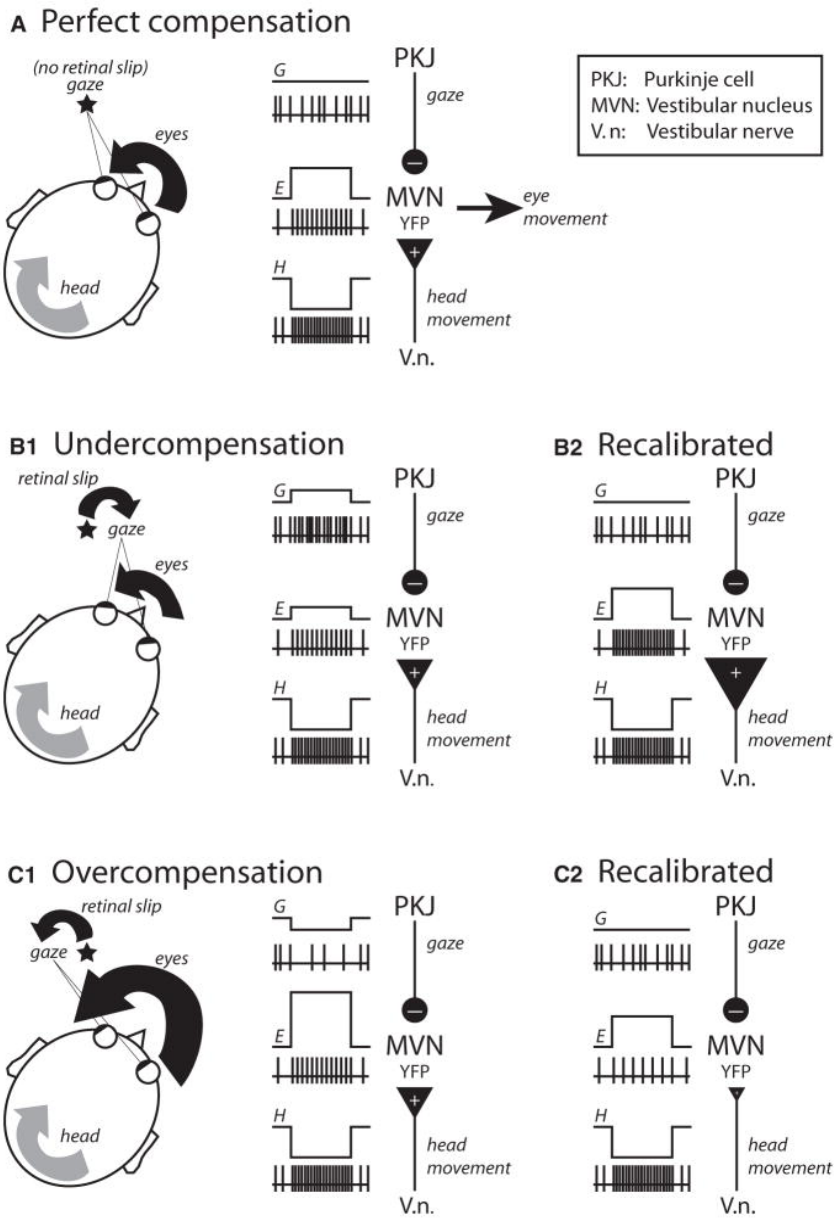

Figure 2 I The Miles and Lisberger Hypothesis. A I The eye movement precisely compensates the head movement in the opposite direction and there is no retinal slip**. B** I (1) In the undercompensation situation, the eyes move less than they are should. (2) The resulting increased firing rate of Purkinje cells leads to the induction of LTP of vestibular nerve synapses in MVN of brainstem (shown by big vestibular nerve synapse) and the output of MVN is increased. As a result, the VOR is recalibrated. **C** I (1) For overcompensation, the eyes move larger than they are should. (2) The resulting decreased activity of Purkinje cells causes LTD of the vestibular synapses (shown by small vestibular nerve synapse) and the output of MVN is decreased. Thus, the VOR is calibrated again.

in the undercompensation situation (Figure 2B), increased firing rate of Purkinje cells leads to the induction of LTP in vestibular nerve synapses in the MVN of brainstem (shown by larger vestibular nerve synapse in Figure 2B2); and for overcompensation, the decreased activity of Purkinje cells causes LTD in the vestibular synapses (shown by smaller vestibular nerve synapse in Figure 2C2). These changes in the strength of the vestibular nerve synapse lead to a larger or smaller eye movement in response to head movement, and therefore calibrate the gain of the VOR.

Direct support for this hypothesis was missing until McElvain et al. (2010) first proved the vestibular nerve synapses in the MVN are plastic. In their experiments, when pairing vestibular nerve stimulation with different postsynaptic membrane potentials of the MVN neurons, bidirectional plasticity is induced in vestibular nerve synapses: LTP was induced when pairing vestibular nerve stimulation with hyperpolarisation (increased Purkinje cells activity in vivo in Figure 2B); and LTD was induced by vestibular nerve stimulation alone (decreased Purkinje cells activity in vivo in Figure 2C). Similar results were obtained by Menzies et al. (2010), confirming the hyperpolarisation mediated plasticity in the vestibular nerve synapse.

It has thus been established that the vestibular nerve synapse is plastic and under what circumstances. But questions arise relating to the underlying cellular and molecular mechanisms of this hyperpolarisation mediated bidirectional plasticity that drives motor learning. To address these questions, computational modelling of the experimental results of McElvain et al. (2010) and Menzies et al. (2010) is a good choice.

1.3 Computational Modelling

Computational modelling is the use of mathematical models based on computer science and physics to investigate the behaviour of complex systems by computational simulation (National Institute of Biomedical Imaging and Bioengineering 2013). Simulations are done by setting different parameters that characterise the system, and analysing the patterns of predicted outcomes. There are many advantages to using a computational model. First, a computational model can simulate a situation when real experiments are constrained. Second, a model can validate a hypothesis based on the actual experimental data. Third, a model can predict the behaviour of the system under normal and disturbed conditions, and provide guide for experiments. Fourth, the computer can handle very complex mathematical relationships quick and accurately, which would take too long to calculate by hand (Psychwiki.com 2016).

The development of numerous methods for biological system modelling has been triggered by two significant advancements (Kotaleski & Blackwell 2010). One advancement is computational capability. A relatively cheap but powerful computer is essential for a temporal and spatial model with thousands of components, which can require trillions of calculations. The second advance is the availability of abundant qualitative and quantitative experimental data, which provides temporal and spatial information about components as well as their relationships and interactions.

1.3.1 Computational modelling in synaptic plasticity

Computational modelling in neuroscience has made great progress in understanding the nature of neurons' behaviour - an interplay between biochemical networks and electrical activities. Many good models have been created to simulate the activities of ion channels (Hodgkin & Huxley 1952), neuron morphology (Rall 1959), neural circuits (Fujita 1982) and network of biochemical signalling pathways (Bhalla & Iyengar 1999). These models can advance our understanding of neural behaviours. For hyperpolarisation mediated synaptic plasticity in the VOR, computational models can do validation and prediction to help describe structure of the VOR neural circuit, provide understanding of specific ion channels' and proteins' function in the molecular mechanism of hyperpolarisation mediated synaptic plasticity, and guide researchers to the most valuable experiments.

Generally, there are two kinds of models for synaptic plasticity: phenomenological and mechanistic. Phenomenological models link neural activity and the resulting synaptic plasticity (Shouval et al. 2002; Song et al. 2000; van Rossum et al. 2000; Pfister & Gerstner 2006; Morrison et al. 2008;). They can precisely trace the resulting changes of synaptic plasticity when changing the behaviour of neural network, but they do not describe the underlying molecular mechanism. In contrast, mechanistic models describe not only electrical activity by classical compartmental models but also biochemical processes, like the calcium dynamics (Holmes & Levy 1990; Schiegg et al. 1995; Gamble & Koch 1987; Zador et al. 1990) and recently, protein signalling cascades (Abarbanel et al. 2002; Shouval et al. 2002; Pi & Lisman 2008; Urakubo et al. 2008) in the form of kinetic equations. Those models were excellent at exploring and describe the quantities and signalling cascades in synaptic plasticity based on the known biochemical pathways and parameters, but they used did not always follow the laws of chemistry (Saudargienė & Graham 2015).

Considering the complexity of interactions between neurotransmitters, neurotransmitter receptors, membrane potential, ion channels, Ca^{2+} dynamics and signalling pathways, a multi-scale computational model is required to explain the cellular and molecular processes underlying this novel neuronal plasticity. Such model should integrate compartmental models which describe the synaptic, electrical activities and Ca^{2+} dynamics of vestibular nucleus neurons, and biochemical models that contain signalling pathways underlying synaptic plasticity. For hyperpolarisation mediated synaptic plasticity in the VOR, there have been models that describe its electrical properties. A compartmental model that studies ionic current and Ca^{2+} dynamics in hyperpolarisation dependent LTD in the MVN has been created by Graham et al. (2009). But biochemical modelling is a relatively novel method to study synaptic plasticity and there is much room for investigation. Comprehensive biochemical models of synaptic plasticity are in great demand.

1.3.2 Biochemical Modelling of Synaptic Plasticity

Biochemical modelling in a quantitative kinetic way is a natural representation of molecular networks, which applies systems theory to chemical kinetics (Le Novère 2015). Biochemical systems consist of the molecular species and interactions between them, and are characterised by quantities of individual species, timing and rate of every interaction. Such models can address fundamental questions. For instance, one model can determine whether the behaviour of the model that is based on the known kinetics support the experimental observations and investigate the role of particular molecules. Such models will lead to a deeper understanding of the molecular mechanisms underlying hyperpolarisation mediated synaptic plasticity.

Two essential advancements have recently promoted the development of synaptic biochemical models. The first is the progress of knowledge about the biochemical signalling underlying synaptic plasticity. Biochemical and cellular activities follow chemical and physical principles. Thus, based on the thermodynamics and chemical kinetics, the gain of parameters of underlying plasticity processes can help us predict the behaviour of the system. The second is the software environment. Once the parameters of the synaptic plasticity system are set, the whole process can be simulated by calculating the changes in variable quantities of each species, such as concentration, over fixed intervals. There have been numerous available tools (Calzone et al. 2006; Keller et al. 2013; Funahashi et al. 2003; Hoops et al. 2006; Takahashi et al. 2004; Myers et al. 2009) for quantitative kinetic modelling in which a user can set up models and simulate their behaviours.

A variety of models have been created to study synaptic plasticity on the basis of following theory: LTP and LTD as two main forms of synaptic plasticity, are induced by postsynaptic Ca^{2+} elevation via the activation of CaMKII and calcineurin (McGlade-McCulloh et al. 1993; Lledo et al. 1995; Mulkey et al. 1994). There are a set of models that studied calcium sensitivity of CaMKII (Michelson & Schulman 1994; Coomber 1998; Kubota & Bower 2001; Pepke et al. 2010). An allosteric model of calmodulin activation has been proposed (Stefan et al. 2008). Spike pattern dependent postsynaptic bidirectional plasticity has been investigated (Bhalla 2002; D'Alcantara et al. 2003; O'Connor et al. 2005; Zhabotinsky et al. 2006; Urakubo et al. 2008) and the dependence of calmodulin activation on calcium influx frequency has been discussed (Franks et al. 2001; Naoki et al. 2005). All of these models show limitations either because of simplification or lack of certain processes, but each of them reflects some properties of the pathway and contributes to the relative complete model of Li et al. (2012).

The Li model (Li et al. 2012) is one of the most complex and complete, and is represented in the Figure R1. The influx of calcium from the ion channels was modelled according to experimental measurements (Sabatini et al. 2002). Calcium then binds calmodulin. The activation of calmodulin by calcium is based on an allosteric model (Stefan et al. 2008), where the calmodulin is in either the open (R) or the close (T) state and has four binding sites with different dissociation constants that are also distinct in the two states. The R conformation of calmodulin is the active state and it can activate either the CaMKII pathway or the calcineurin pathway. In the CaMKII pathway, the CaMKII in the CaMKII/calmodulin complex can be phosphorylated on Thr286 by autophosphorylation and thereby is activated. Subsequently, phosphorylated CaMKII and CaMKII/calmodulin complex can both phosphorylate the GlunR1 subunit of AMPA receptors, leading to an enhanced function of AMPARs. In the calcineurin pathway, calcineurin first binds four Ca^{2+} to activate its catalytic subunit and the activated calcineurin can associate with Ca^{2+}-calmodulin (Klee et al. 1998). Then the calcineurin/calmodulin complex dephosphorylates DARPP-32. DARPP-32 can inhibit (Protein phosphatase 1) PP1 and PP1 can dephosphorylate AMPAR. As a result, activation of this pathway dephosphorylates AMPARs and leads a weakened function of AMPARs.

Here, I combined the detailed biochemical network model based on Li et al (2012) on a larger temporal scale with the electrical model of MVN neurons, to investigate the possible mechanisms involved in hyperpolarisation dependent synaptic plasticity in the MVN. I implemented the stimulation protocols that induced vestibular synapse bidirectional plasticity in the electrical model of MVN B neuron (McElvain et al 2010), investigated the

relationship between Ca^{2+} influx and different patterns of synaptic activity, and analysed the relationship of AMPA receptor phosphorylation ratio with the Ca^{2+} dynamics induced by the different patterns of synaptic activity.

2 Methods

2.1 Models

2.1.1 Electrical model of MVN type B neuron

The electrical model I used in the project is a multiple compartment model of guinea-pig media vestibular nuclei type B neurons that was adapted from Quadroni & Knöpfel's model (1994). The model structure and the parameters fit the well-characterised behaviours of type B MVN neurons in electrophysiological recordings.

The model has 4 identical branched proximal dendrites and each branch of proximal is followed by 2 branches of distal dendrites. Every proximal dendrite consists of 3 electrical compartments and every distal dendrite consists of 6 compartments; The total number of electrical compartments is 61.Each electrical compartment contains three neurotransmitter receptors and up to nine active ionic channels: NMDA receptor AMPA receptor and GABA (gamma-aminobutyric acid) receptor, fast inactivating sodium channel (Na), persistent sodium channel (Nap), low-voltage activated calcium channel (Ca(LVA) or LVACC), high-voltage activated calcium channel (Ca(HVA) or HVACC), fast-voltage activated potassium channel (K(fast)), slowly relaxing voltage activated potassium conductance (K(slow)), fast transient potassium channel (K(A)), slowly relaxing mixed sodium-potassium channel activating at hyperpolarised membrane potentials (H), and calcium-activated potassium channel (K(AHP)). The weight of NMDAR, AMPAR and GABAR are 2e-5, 5e-5 and 0.05, respectively. The kinetic parameters, distribution and density of channels are listed in appendix table 1 and 2. The Ca^{2+}-pump and Na^{+}-Ca^{2+} exchanger are used to model the intracellular free [Ca^{2+}] current. The electrical compartment was modelled by 25 and 6 shell-like compartments respectively in the soma and proximal dendrites for calcium diffusion within compartment.

The electrical model was built and run in NEURON (Carnevale & Hines 2006). I am grateful to Prof Bruce Graham (Stirling University) for kindly providing the basic scripts implementing this model in NEURON.

2.1.2 Biochemical model of signalling pathways underlying synaptic plasticity

The biochemical model used here is based on Li et al. (2012) model and is of the signalling pathways underlying synaptic plasticity; starting from Ca^{2+} to phosphorylated AMPARs. There are a total of 129 molecular species and 678 reactions in the model. Initial concentrations of species are listed in appendix table 3. The files describe the detailed

information such as species names, reactions and reaction kinetic parameters is in Dropbox, whose link is in the supplementary information.
The biochemical model was edited and run in COPASI(Hoops et al. 2006). And it is available in COPASI (.cps) and SBML level 2.4 (.xml) format.

2.2 Simulation Protocol

2.2.1 Simulation in Electrical model

The electrical model was run for 1000 ms before applying synaptic activities, in order to achieve its initial equilibrium state. presynaptic excitatory (AMPA-NMDA glutamatergic) and inhibitory (GABAergic) stimulations were applied to mimic the stimulation protocols used by McElvain et al (2010) to induce LTP or LTD. The excitatory stimulation comprised of 550 ms activation of AMPA receptors and NMDA receptors activation at 100 Hz. The inhibitory input comprised of 250 ms GABA receptor activation at 100 Hz, which started simultaneously with the excitatory stimulation (see Figure R8A and B).

2.2.2 Simulation in Chemical model

2.2.2.1 Parameter scan

The “Parameter Scan” function in COPASI was used to explore the relationship between Ca^{2+} concentration and AMPARs phosphorylation ratio. The scan object is initial Ca concentration, which in fact is fixed at initial value during the whole simulation. The minimum concentration is 3e-10 M and the maximum concentration is 3e-7 M with 59 logarithmic intervals. Each task in the scan starts from the initial state of the biochemical model and runs for 800 s with the interval size being 0.0001 s.

2.2.2.2 Stabilization

Before applying the synaptic activities to the neuron model, I used the Ca^{2+} dynamics from the spontaneously firing neuron to stabilise my biochemical system. The stabilization protocol was first run for 400 s with interval size being 0.0001 s. After updating the model and saving the file, the model was run for another 400 s.

2.3 Multi-scale Modelling

Intracellular calcium concentration is modelled in the electrical model by NEURON as a result of interaction between membrane potential, ion channel conductances, synaptic activities and NMDA receptor activation. I output the Ca^{2+} profile from NEURON with time resolution 0.025ms in a text format file. Then I used a Python script (in supplementary information) to translate the electrical Ca^{2+} signal to provide an input of Ca^{2+} to the chemical

model. In the script, the total intracellular calcium concentration was scaled by a factor of 1/50 to give the Ca^{2+} concentration for my biochemical system. To adjust the time resolution from 0.025 ms to 1 ms, which is appropriate for chemical reactions and also speeds up the simulation, I calculate the average Ca^{2+} concentration every 40 values. Those values were translated into the COPASI event language, which later are put in the COPASI file behind content “</ListOfReactions>” and before content “<ListOfModelParameterSets activeSet=”ModelParameterSet_0”>”. Finally, I ran the chemical mode.

3 Results

3.1 Characterization of Biochemical Model of Bidirectional Plasticity

3.1.1 Description of key events in the model

The key molecular species and reactions between them that underlie synaptic plasticity are represented in Figure R1, which was created by us using the process diagram language of System Biology Graphical Notation (Le Novère et al. 2009). This biochemical network was based on the model developed by Li et al. (2012). The model of Li et al was extended by adding the Ca^{2+}-dependent activation of PP2Bi and the missing reaction (CamR_Ca2_AC + PP2B -> CamR_Ca2_AC_PP2B). The extended model was translated into COPASI format and the model description file is available on Dropbox (supplementary information). The biochemical network can be divided into five parts: the input (yellow), the phosphorylation signalling pathway (red), the dephosphorylation signalling pathway (blue), the anti-dephosphorylation pathway (pink) and output (shown in green). Ca^{2+} (shown in yellow) is the original input of system and therefore, to some degree, it controls the whole system. The source of Ca^{2+} is the voltage-dependent calcium channel and NMDA receptors, as a result of interactions between membrane potential and ion channels, synaptic activity and neurotransmitter receptor activation. After influx, Ca^{2+} binds and activates calmodulin. Active calmodulin can activate both CaMKII and calcineurin, and therefore introduces a competition that determines the relative activation ratio of these two species. The AMPARs phosphorylation ratio represents the synaptic strength: an increase in the ratio leads to synaptic potentiation and a decrease leads to synaptic depression. CaMKII and calcineurin have opposing effects on the phosphorylation of AMPA receptors. CaMKII is active when it is phosphorylated, bound to calmodulin, or both. Active CaMKII can autophosphorylate unphosphorylated CaMKII as well as phosphorylate AMPARs. The calcineurin-calmodulin can dephosphorylate DARPP-32 and therefore stops it from inhibiting PP1. The active PP1 can directly dephosphorylate AMPARs. To sum up, concentration of Ca^{2+} and calmodulin influences the competition of active calmodulin between CaMKII and calcineurin, which late determines the active amount of CaMKII and PP1, and consequently regulates the AMPARs phosphorylation ratio.

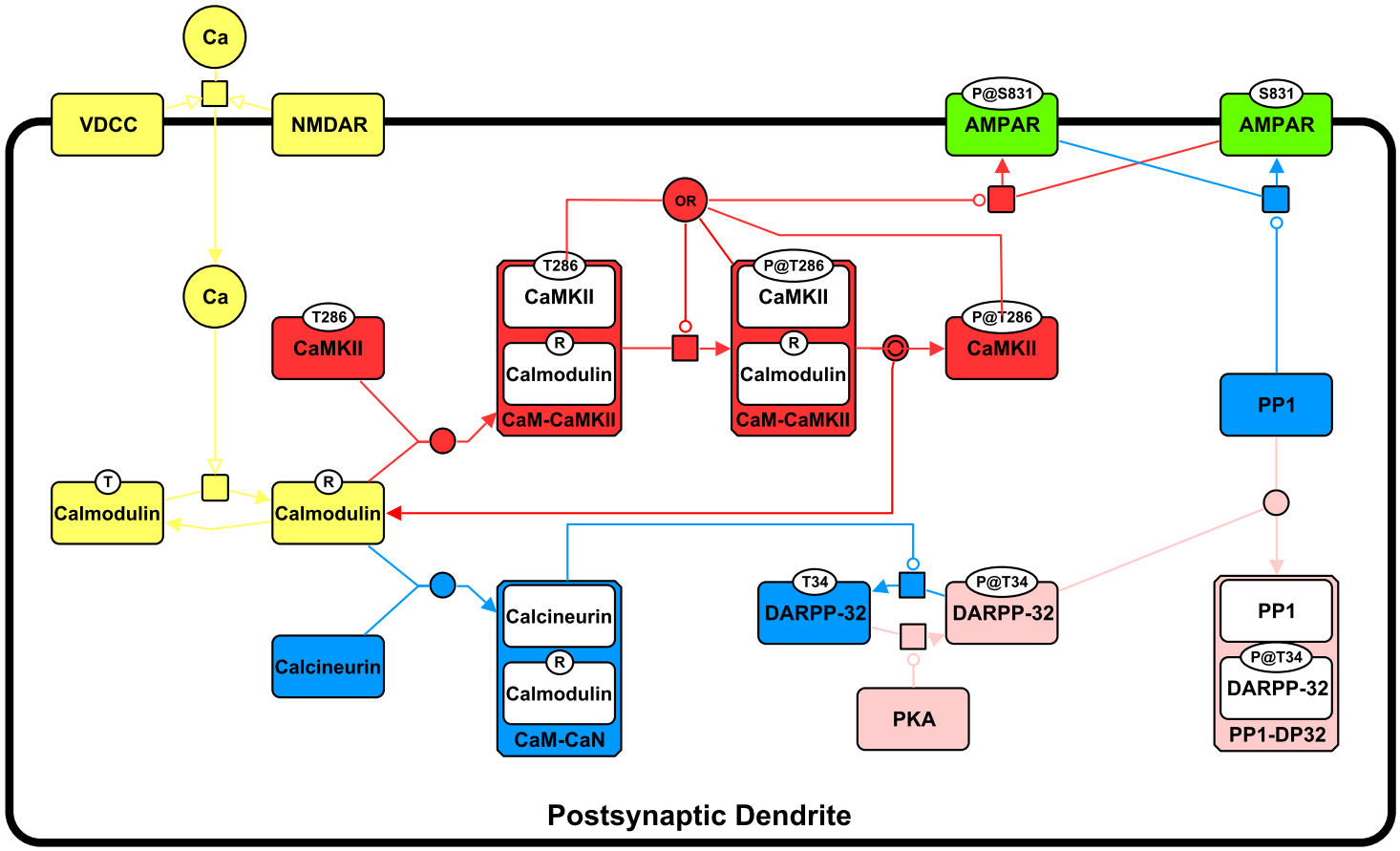

Figure R1. Simplified schematic diagram of signalling pathways underlying bidirectional plasticity. Ca^{2+}, the input of system, inflows through VGCCs and NMDA receptors and then activates calmodulin (the yellow part). The R state calmodulin activates either CaMKII pathway (the red part) or calcineurin pathway (the blue part). In the CaMKII pathway, the CaMKII-calmodulin complex, phosphorylated CaMKII-calmodulin complex and phosphorylated CaMKII are the active forms of CaMKII. They can phosphorylate the inactive CaMKII as well as AMPAR, leading to an enhanced function of AMPAR. In the calcineurin pathway, the calcineurin-calmodulin complex dephosphorylates DARPP-32, and thereby releases PP1 from inhibition. Active PP1 can dephosphorylate AMPAR, leading a weakened function of AMPARs. The PKA pathway (the pink part) can reduce the dephosphorylation activity by activate DARPP-32.

3.1.2 Relationship between Ca^{2+} concentration and AMPAR Phosphorylation Ratio

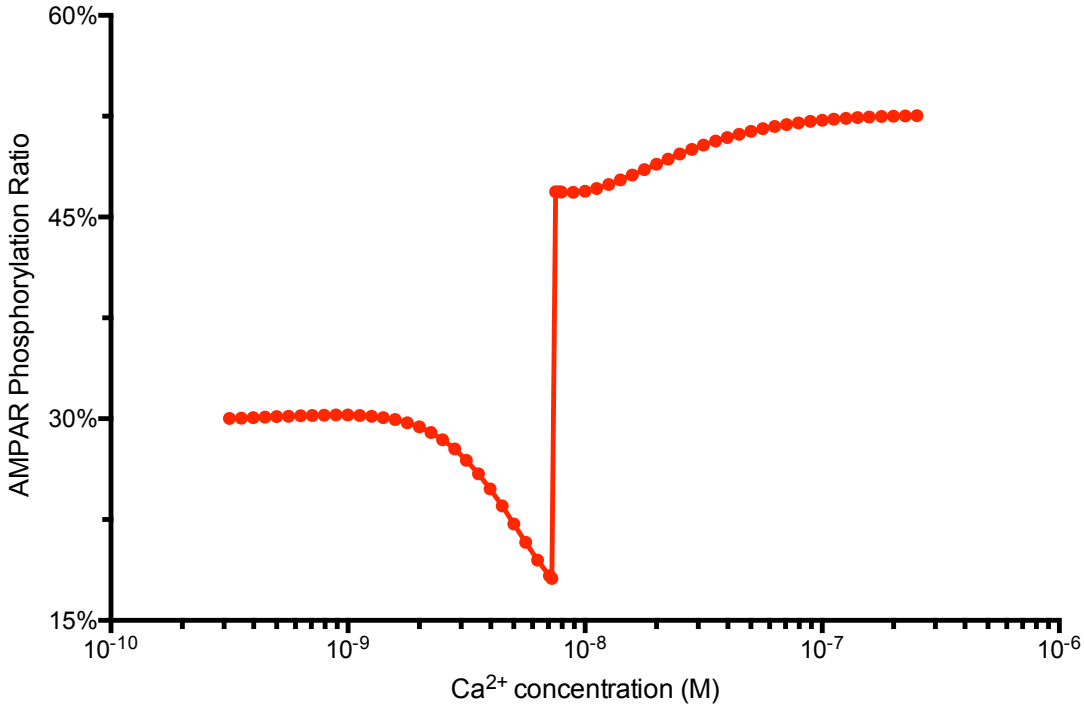

Figure R2. Complex relationship between Ca^{2+} concentration and AMPAR phosphorylation ratio. The steady value of AMPAR phosphorylation ratio is recorded at different fixed Ca^{2+} concentrations.

As described above, the amount of intracellular Ca^{2+} indirectly controls the phosphorylation ratio of AMPAR. It has been reported that moderate elevations of Ca^{2+} concentration cause relatively more dephosphorylation of AMPARs, resulting in a decrease in synaptic weight while substantial elevations of Ca^{2+} concentration cause relatively more phosphorylation of AMPARs, resulting in an increase in synaptic weight (Lisman 1989). To systemically and quantitatively reveal the relationship between Ca^{2+} concentration and AMPAR phosphorylation, I scanned a large range of Ca^{2+} concentrations and recorded the steady value of AMPAR phosphorylation ratio. As shown in the Figure 2R, the relationship between Ca^{2+} concentrations and AMPAR phosphorylation ratio is complex. Raising Ca^{2+} concentration from resting value of 10^{-9} M to a level around 7.25×10^{-9} M, there is a progressive decrease in the AMPAR phosphorylation ratio. This indicates that a moderate increase of Ca^{2+} concentration, in this case, lower than around 7.25×10^{-9} M, which occurs at anti-Hebb conditions, does cause synaptic depression; and a large increase of Ca^{2+} concentration, larger than 7.52×10^{-9} M, which occurs at Hebb conditions, causes a significant increase of AMPAR phosphorylation ratio and results in synaptic potentiation.

What makes the result more exciting is that a bistability is observed here, which is perfect for explanations of bidirectional plasticity. When Ca^{2+} concentration is 7.25 x 10^{-9} M, the AMPAR phosphorylation is 18.12%. While Ca^{2+} concentration is 7.52 x 10^{-9} M, the AMPAR phosphorylation jumps to 46.88%. This indicates that there is a biochemical trigger in this system that has the potential to directly control the bidirectional plasticity of AMPA receptors and synaptic plasticity in these neurons.

3.1.3 The Kinetic Mechanisms of Bidirectional Plasticity

To deepen the mechanistic understanding of how different Ca^{2+} elevations trigger the bidirectional plasticity, the steady active CaMKII ratio, active PP1 ratio and their ratio, which respectively represents the phosphorylation and dephosphorylation strength of AMPAR, are plotted under Ca^{2+} concentration conditions in Figure R3. In the “depression” range of Ca^{2+} concentration, the activation rate of PP1 is higher than CaMKII. This can be accounted by different affinity of calcineurin and CaMKII to calmodulin, which was demonstrated to be important for the ability of calmodulin to act as a calcium-dependent switch by Stefan et al. (2008): calcineurin have stronger affinity to calmodulin than CaMKII.

However, when the Ca^{2+} concentration is higher than the “trigger value” and is in the potentiation induction range, the active CaMKII ratio increases rapidly. To understand this, the proportion of two types of active CaMKII in different level of high Ca^{2+} concentration is displayed in the Figure R4 A. Notably, the proportion of phosphorylated CaMKII increases a little in the depression condition but is greatly increased when the Ca concentration increases to potentiation condition. The autophosphorylation of CaMKII is the reason, as shown in Figure R4B. The autophosphorylation rate quickly increases when the active CaMKII ratio is higher than around 16% and therefore a positive feedback loop is formed. This is biologically reasonable. CaMKII is a dodecamer with 12 identical subunits arranged in two rings of six subunits each. Phosphorylation happens between neighbouring subunits on the same ring. Once around 16% of CaMKII is activated, this means that at least one subunit is active in average in each hexametric ring. This active subunit can then act as a catalyst to phosphorylate neighbouring subunits once they bind to calmodulin. A persistent activation then is achieved by this “chain reaction”. This result is consistent with my observation in active CaMKII ratio – [Ca^{2+}] scanning, where the active CaMKII ratio starts to increase dramatically when Ca^{2+} concentration is high enough to form a powerful positive loop. These results show that the induction of depression period is due to different affinities of CaMKII and calcineurin, while potentiation period is induced by the persistent activation of CaMKII autophosphorylation.

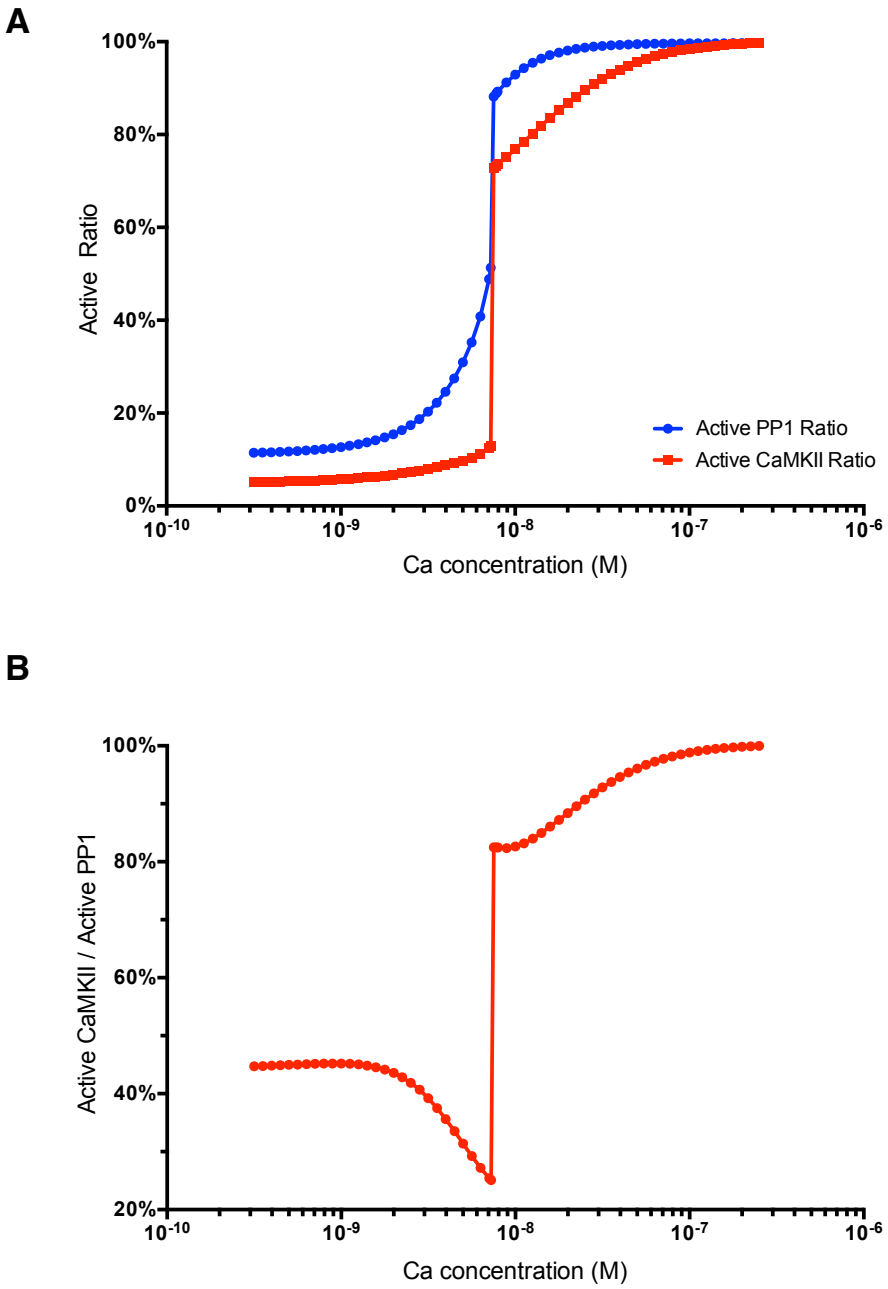

Figure R3. Kinetic mechanisms behind Ca^{2+}-dependent Bidirectional plasticity. (A) Activation of CaMKII and PP1 over a range of Ca^{2+} concentration. (B) The ratio between active CaMKII ratio and active PP1 ratio over a range of Ca^{2+} concentration. Each point represents one simulation.

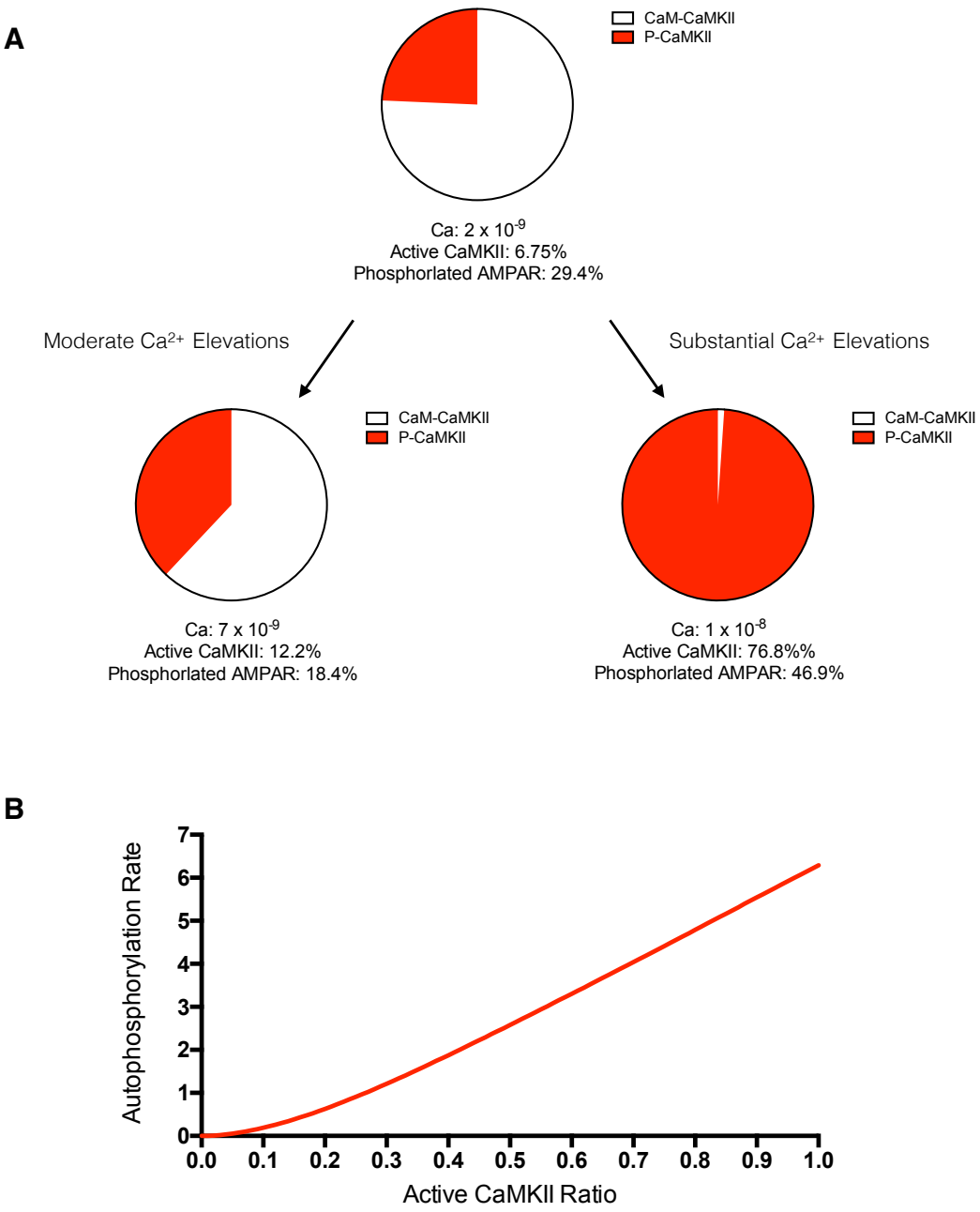

Figure R4. Role of CaMKII autophosphorylation in the bidirectional plasticity. (A) The proportion of CaM-CaMKII and phosphorylated CaMKII when Ca^{2+} concentration is 2 x 10^{-9} M (upper), 7 x 10^{-9} M (left) and 1 x 10^{-8} M (right). (B) The relationship between autophosphorylation rate and active CaMKII ratio.

3.1.4 Effect of Ca^{2+} concentration elevation duration on AMPARs Phosphorylation Ratio

Besides the level of Ca^{2+} elevations, the duration of Ca^{2+} elevations are important for bidirectional plasticity since the biochemical processes are relatively slow and it takes minutes to reach a new steady state. To investigate the effect of Ca^{2+} elevation duration on AMPARs phosphorylation ratio, the time course of Ca^{2+} concentration elevation during depression and potentiation are plotted in the Figure R5. Different Ca^{2+} concentration elevations are applied on the steady state where Ca^{2+} concentration is 2×10^{-9} M and AMPAR phosphorylation ratio is 29.4%. For the depression condition, the Ca^{2+} concentration is elevated to 4×10^{-9} where AMPAR phosphorylation ratio is 24.7%. The value of AMPARs phosphorylation ratio increases for around 10 s before decrease to a steady state at around 200 s. For the potentiation condition, the Ca^{2+} concentration is elevated to 1×10^{-8} M where AMPAR phosphorylation ratio is 46.6%. The value of AMPARs phosphorylation ratio increases for around 7 s before decrease to 26.4% at 30 s, and then it rises to a steady state at around 300 s. After 10 s in depression and 30 s in potentiation condition, the degree of depression and potentiation is progressively enhanced. This suggests that the degree of synaptic strength change is time dependent: in a certain range, the longer the Ca^{2+} elevations last, the stronger the strength changes, which is reasonable.

However, the unstable states before continual decline and rise in both the depression and potentiation condition are unexpected. The proportion of active CaMKII, PP1 and their ratio is plotted with time to study the kinetic mechanisms. In the Figure R5 (C, D). The proportion of active CaMKII shows a quicker increase than PP1 at the beginning in both conditions. This indicates that active CaMKII, which phosphorylates AMPAR is more sensitive than active PP1, which dephosphorylates AMPARs, to Ca^{2+} concentration changes. As time goes on, the proportion of active PP1 keeps increasing while that of active CaMKII slows down in the later phase of the depression condition and middle of potentiation condition. For the later phase of the potentiation condition, the rapid increase of CaMKII autophosphorylation strongly elevates the proportion of phosphorylated AMPAR induced by the same mechanism described in Figure R4.

In conclusion, the changes of phosphorylated AMPAR proportion during Ca^{2+} concentration elevations are time dependent. In the early period of depression and potentiation, the CaMKII is more sensitive to Ca^{2+} than PP1 and thus an increase of phosphorylated AMPAR proportion is introduced. In the middle period of potentiation and the later period of depression, the increase of rate of active CaMKII proportion slows down while the increase

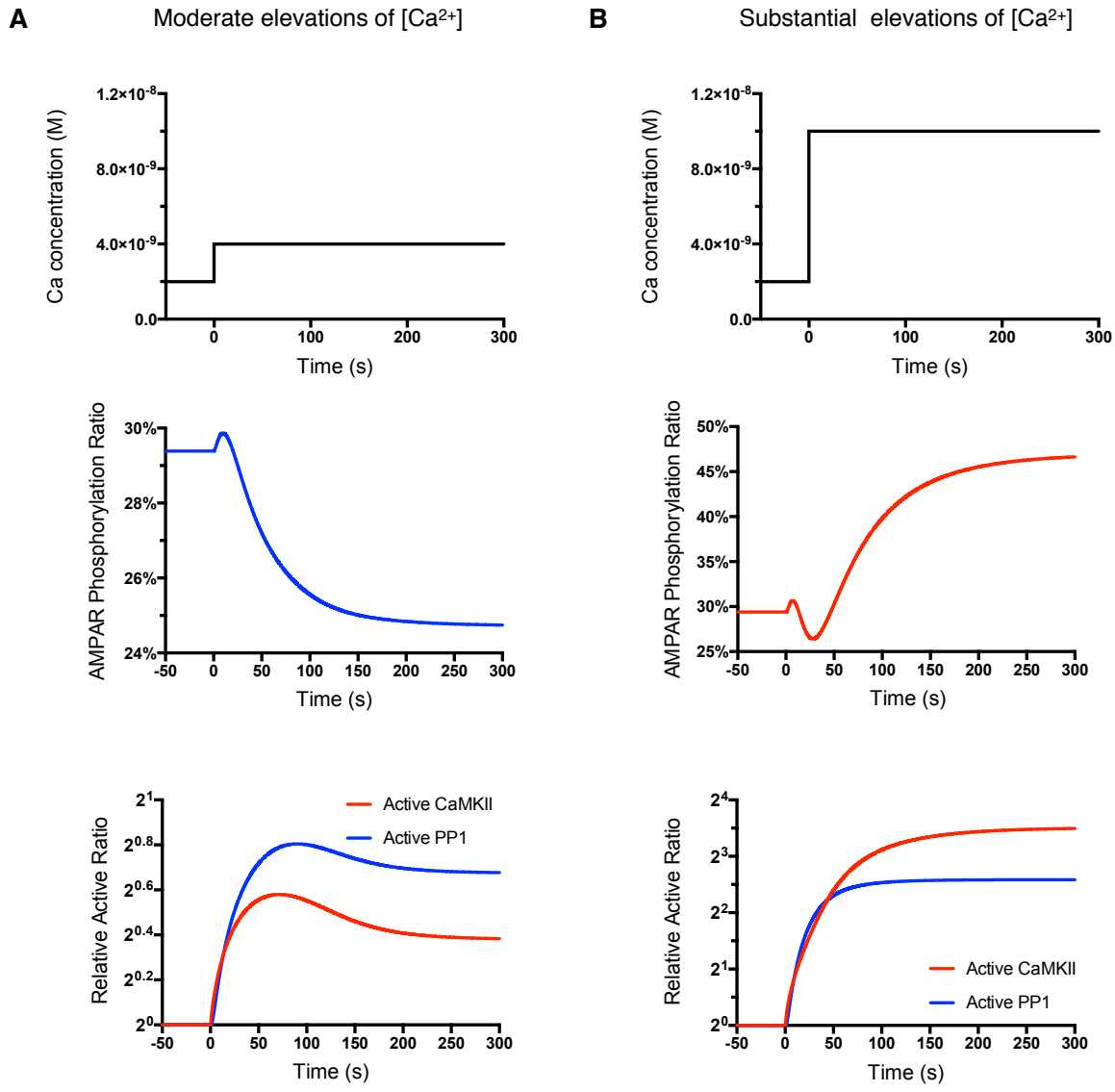

Figure R5. The time course of AMPAR phosphorylation ratio after Ca^{2+} concentration elevations. The time courses of Ca^{2+} concentration(left), AMPAR phosphorylation ratio (middle), CaMKII (red) and PP1 (blue) relative active ratio (right) with moderate (A) and substantial (B) Ca^{2+} concentration elevations at 0 s. Relative active ratio = transient active ratio / initial active ratio.

rate of active PP1 proportion keeps at a relative high level, which then makes the dephosphorylation activity stronger than phosphorylation activity and results in a decrease of phosphorylated AMPAR proportion. In the later period of the potentiation condition, the active CaMKII proportion reaches a range where the autophosphorylation rate of CaMKII suddenly increases. Then the fast-rising of active CaMKII proportion causes a net of phosphorylation of AMPAR and results in a fast and progressive increase of phosphorylated AMPAR ratio.

3.1.5 Role of Calmodulin in AMPAR Phosphorylation Ratio

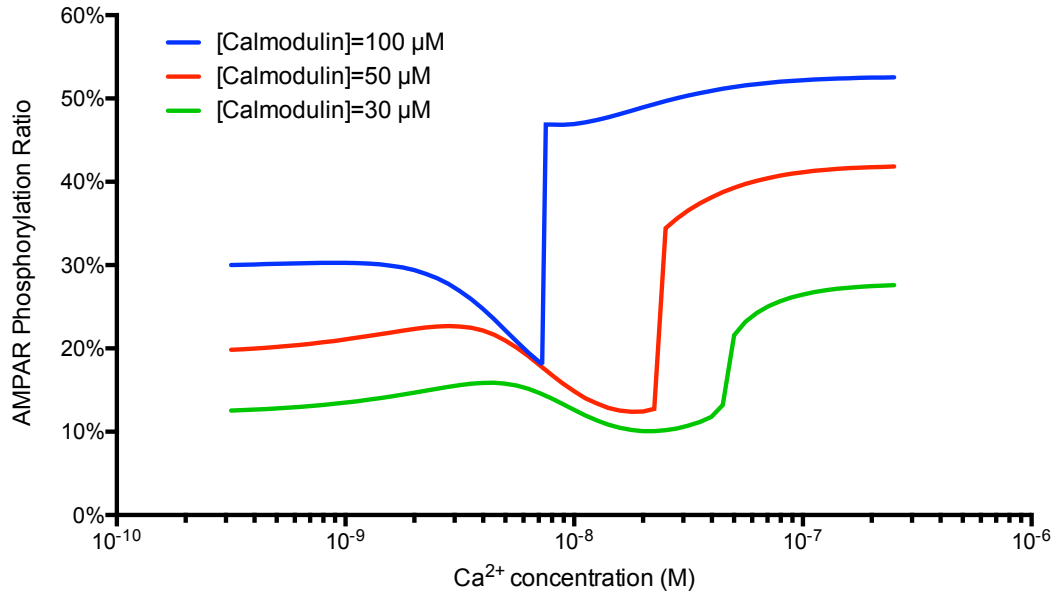

Figure R6. Effect of calmodulin concentration on phosphorylation of AMPAR and relative activation of CaMKII and PP1. The relationship between steady AMPAR phosphorylation ratio and Ca^{2+} concentration is plotted for initial calmodulin concentrations of 100 μM, 50 μM and 30 μM condition.

Calmodulin is the intermediate protein which links calcium to CaMKII and calcineurin. Thus the concentration of calmodulin affects the sensitivity of CaMKII and calcineurin towards Ca^{2+}, which therefore influence the phosphorylation and dephosphorylation activity of AMPARs. To fully understand the role of calmodulin in this system, a range of physiological calmodulin concentrations (Cimler et al. 1985; Gamble & Koch 1987; Biber et al. 1984) was tested. Figure R7 represents the relationship between phosphorylated AMPAR ratio and Ca^{2+} concentration with 30, 50, 100 μM calmodulin. When Ca^{2+} concentration is low, the increase of calmodulin concentration elevates the AMPAR phosphorylation ratio. When Ca^{2+} concentration is in the range where bidirectional plasticity is induced, an earlier and

faster induction of synaptic potentiation is observed in higher calmodulin concentration. To understand the underlying mechanisms, the ratio of active CaMKII to active PP1 is plotted over time with the corresponding calmodulin concentration. A relatively earlier activation of CaMKII than PP1 is observed, which can be explained by increased free active calmodulin and can explain the earlier activation of synaptic potentiation. This result shows that the biochemical system with 100 μM calmodulin has a more sensitive activation bi-stability and therefore this concentration of calmodulin has been applied for my future studies.

3.2 Characterization of Electrical Model

3.2.1 Description of Electrical Model

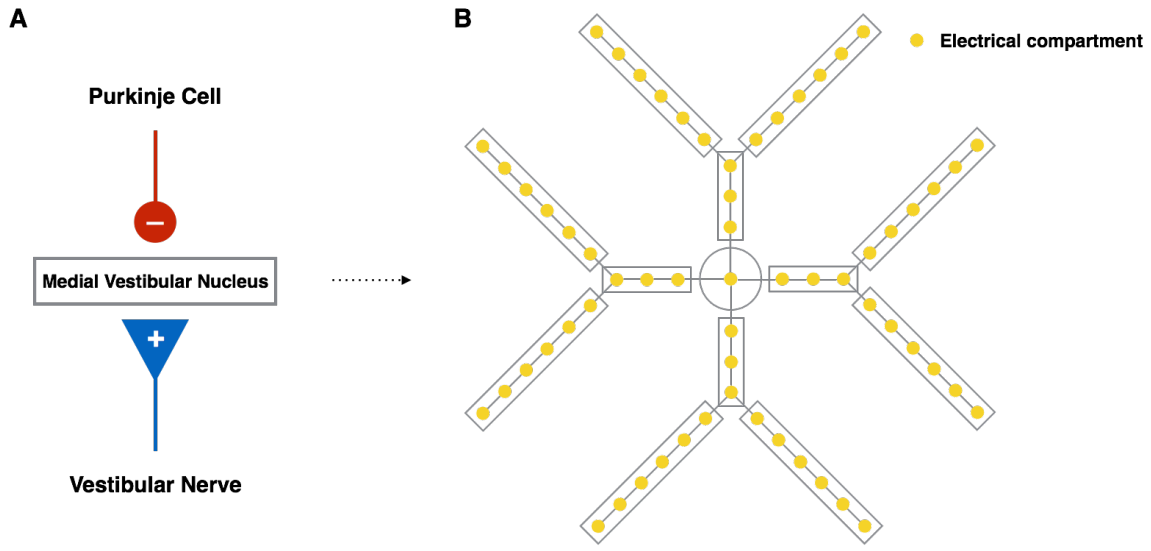

Figure R7. Schematic of the electrical model. (A) Regulation of medial vestibular nucleus (MVN) activity. MVN is under regulation of Purkinje cells and vestibular nerves, which respectively inhibit and stimulate MVN. (B) Compartmental diagram of MVN B neuron model. The MVN B neuron in the model is consisted of 1 soma, 4 branches of proximal dendrites with 2 distal branches of distal dendrites each. There are total 61 compartments in this model and except soma, every compartment contains a AMPAR, NMDA receptor and GABA receptor. Ca^{2+}, the bridge to chemical model, is calculated in the electrical model as a result of interaction between membrane potential and VDCCs (HVACC and LVACC), synaptic activities and NMDA receptor activity.

MVN receives signals of head movement through excitatory stimulation of vestibular nerve and receives signals of the object slipping in the retina through inhibitory stimulation from Purkinje cell (Figure R7 A). Bidirectional plasticity in the vesicular nerve synapses was demonstrated as a result of different synaptic activities (McElvain et al. 2010). Ca^{2+}, as descried before, is the key player in the underlying mechanism of bidirectional plasticity. To study how different patterns of synaptic activities affect the [Ca^{2+}] dynamics and therefore induce bidirectional plasticity, an compartmental electrical model of MVN B neuron adapted from Quadroni & Knöpfel (1994) was used. The model was implemented in Neuron by Graham et al. (2009b), who kindly provided the scripts used here for the electrical modelling.

This electrical model of MVN B neuron has 1 soma, 4 branches of proximal dendrites and 8 distal branches of distal dendrites and comprises 61 electrical compartments. In each compartment, there are up to nine active ionic channels. Besides, AMPAR and NMDAR are

included to simulate the excitatory stimulation of vestibular nerve and GABAR are used to simulated the inhibitory stimulation of Purkinje in this model. Detailed description and properties can be found in the methods part. The intracellular [Ca^{2+}] that links electrical model to chemical model, is from VDCCs (HVACC and LVACC), which are controlled by membrane potential, and NMDAR, which is gated by excitatory synaptic activity.

3.2.2 Membrane Potential and [Ca^{2+}] response to different patterns of Synaptic Activities

To study the membrane potential and [Ca^{2+}] response to different synaptic activities, the protocols (McElvain et al. 2010) that respectively induced bidirectional plasticity are implemented here. “Single excitatory stimulation” protocol consisted of 550 ms excitatory stimulation that was simulated by 100 Hz AMPAR and NMDAR activation (Figure R8 A), which induced LTD in McElvain et al. (2010). “Dual stimulation” protocol consisted of 550 ms excitatory stimulation paired with a 250 ms inhibitory stimulation that simulated by 100 Hz $GABA_AR$ activation (Figure R8B). The MVN B neuron was spontaneously firing at around 24 Hz before stimulation. The single excitatory stimulation protocol evoked a firing rate of around 56 Hz and the intracellular [Ca^{2+}] increased to 1.72 times the no-protocol baseline (Figure R8A). The dual stimulation protocol caused around 18 mV hyperpolarisation at the first 250 ms, followed by largely increased firing rate (Figure R8B). Remarkably, following a decrease of [Ca^{2+}], a large rebound of [Ca^{2+}] came at the end of inhibitory stimulation, which elevated the average [Ca^{2+}] during the stimulation to 2.77 times the no-protocol baseline. These data show that the postsynaptic voltage controls the [Ca^{2+}] influx during excitatory stimulation: moderate and substantial [Ca^{2+}] elevations are induced respectively without and with hyperpolarisation.

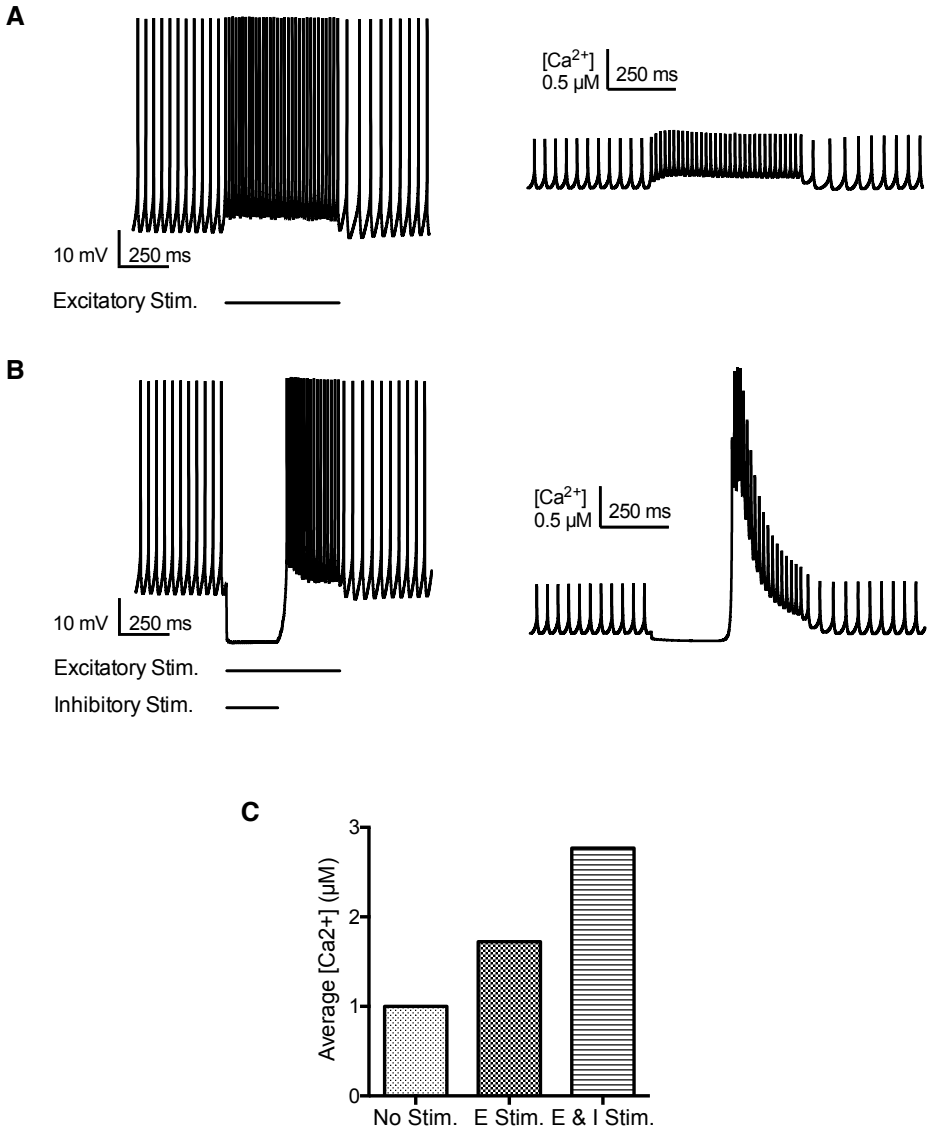

Figure R8. Membrane potential and [Ca^{2+}] dynamics during different patterns of synaptic activities. (A) Membrane potential (left) and [Ca^{2+}] (right) response to protocol comprising 550 ms excitatory stimulation that simulated by 100 Hz AMPAR and NMDAR activation. Elevated firing frequency and moderate [Ca^{2+}] elevations are observed during stimulation. (B) Membrane potential (left) and [Ca^{2+}] (right) response to protocol comprising 550 ms excitatory stimulation that simulated by 100 Hz AMPAR and NMDAR activation and 250 ms hyperpolarisation caused by inhibitory stimulation that simulated by 100 Hz $GABA_AR$ activation. Hyperpolarisation by 18 mV and reduction of [Ca^{2+}] is observed during $GABA_AR$ activation. Elevated firing frequency and huge rebound of [Ca^{2+}] come after hyperpolarisation. (C) Average [Ca^{2+}] is calculated during stimulation (500 – 1050 ms).

3.2.3 Source of intracellular Ca^{2+} during Different types of Synaptic Activities

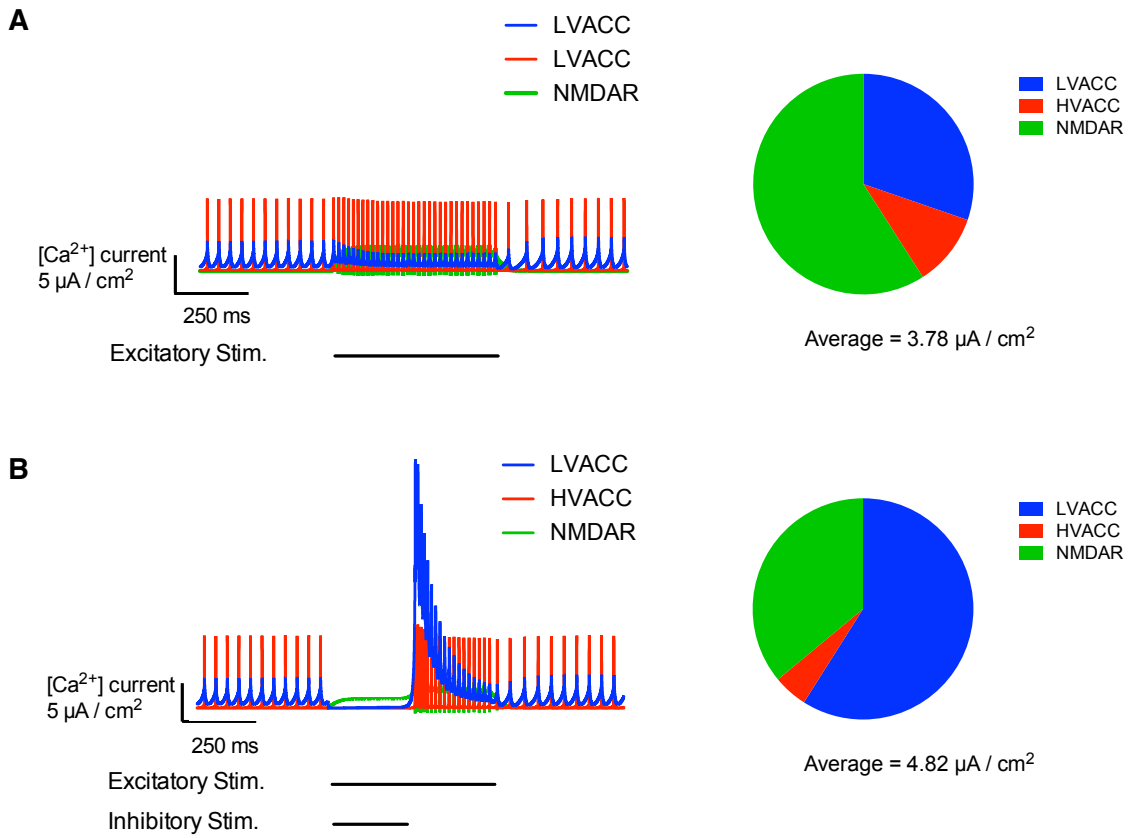

Figure R9. Analysis of Ca^{2+} influx in different synaptic activities. Ca^{2+} influx dynamics over time (left) and contribution of LVA, HVA calcium channel and NMDA receptor to Ca^{2+} influx (right) during different stimulation. (A) Protocol comprises 550 ms excitatory stimulation that simulated by 100 Hz AMPAR and NMDAR activation. (B) Protocol comprises 550 ms excitatory stimulation that simulated by AMPAR and NMDAR activation and 250 ms hyperpolarisation caused by inhibitory stimulation that simulated by 100 Hz $GABA_AR$ activation.

What are mechanisms for different $[Ca^{2+}]$ elevations under different postsynaptic voltage? The intracellular Ca^{2+} is from HVACC, LVACC and NMDAR. Consequently, I assessed the contribution of different sources to intracellular $[Ca^{2+}]$ by observing the dynamics of Ca^{2+} under different synaptic stimulation. In the no-protocol period, the Ca^{2+} is only from LVACC and HVACC with relatively contribution of 5.6:1. During singe excitatory stimulation, the relative contribution of LVACC, HVACC and NMDAR is 2.8:1:5.5, which indicates that NMDAR becomes the main source of Ca^{2+}. Notably, the LVACC dominates the Ca^{2+} influx in the hyperpolarisation involved protocol, with the contribution of LVACC, HVACC and NMDAR being 11.8:1:7.2. These results demonstrate that the activation of NMDAR causes moderate influx of Ca^{2+} and the enhanced activation of LVACC by hyperpolarisation causes

substantial Ca^{2+}. Thus, postsynaptic hyperpolarisation controls the degree of Ca^{2+} influx, which can consequently control the direction of plasticity.

3.3 Multi-scale Modelling of Hyperpolarisation mediated Plasticity

So far, characterization of the relationship between Ca^{2+} concentration and AMPAR phosphorylation ratio and the relationship between the Ca^{2+} dynamics and different patterns of synaptic activities have been described. Next, I link the biochemical model and the electrical model to test my hypothesis that hyperpolarisation during excitatory stimulation can cause substantial elevations of [Ca^{2+}] mainly through LVACC, resulting in synaptic potentiation and excitatory simulation only cause moderate [Ca^{2+}] elevations mainly through NMDAR, resulting in synaptic depression.

3.3.1 Description of Multi-Scale Model

The multi-scale model, which is consisted of the electrical and biochemical model described before, is shown in Figure R10. The electrical model calculates the electrical [Ca^{2+}], which is from LVACC, HVACC and NMDAR, as a result of interactions between ionic channels, membrane potential, neurotransmitters and synaptic activities. After scaling, the Ca^{2+} is output from the electrical model is used as an input to the biochemical model and determines the AMPAR phosphorylation ratio.

3.3.2 Induction of Synaptic Depression *in silico*

Initially, I test whether excitatory stimulation can induce synaptic depression, using the excitatory stimulation protocol that is used by McElvain et al. (2010) to produce LTD. Starting at 0 ms, the 550 ms excitatory stimulation is repeated every 1 second for all the compartments. The Ca^{2+} dynamics in the middle compartment at one of the proximal dendrites (Figure R11), which is characterised in Result 3.2.2, is put into the complex chemical system after being converted to chemical Ca^{2+}. The dynamics of relative AMPAR phosphorylation ratio, which is normalised to the initial value, is shown in Figure 11C over 180 s simulation time. I observed a short (around 10 s) increase of AMPAR phosphorylation ratio, followed by a progressive decrease of AMPAR phosphorylation ratio that reached 0.85 at 180 s. This result confirms that the excitatory stimulation in vestibular synapses can induce synaptic depression.

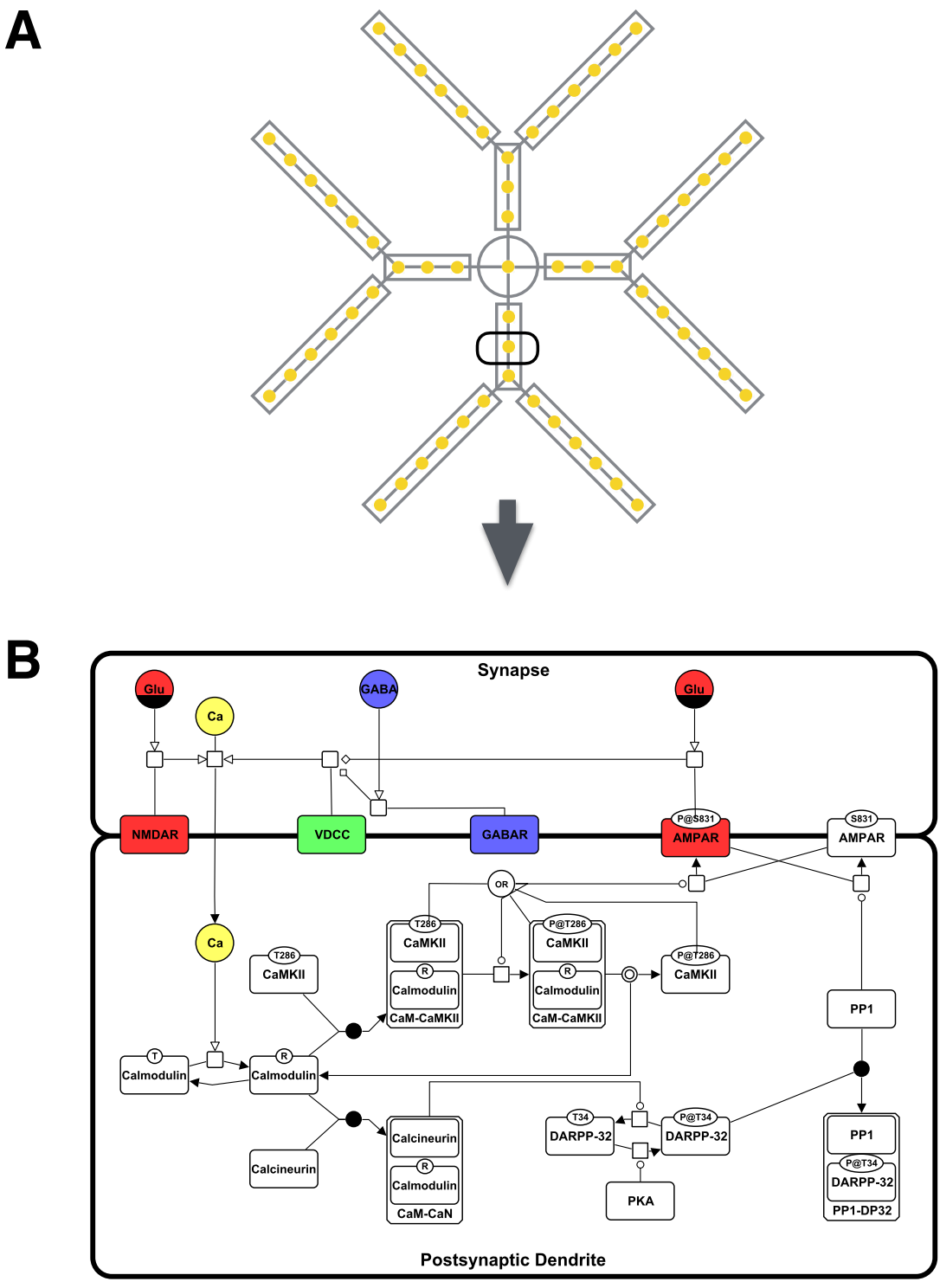

Figure R10. Schematic of the multi-scale model. (A) The activity of the middle compartment in one of the proximal dendrites is recorded. (B) The electrical Ca^{2+} is determined by NMDAR (left, red) as well as VDCCs (green), which can be modulated by AMPAR (right red) and GABAR (blue) in the electrical model. After scaling, the electrical Ca^{2+} generated as output from the electrical model is used as input for the biochemical model. Consequently, a series of reactions are triggered and determine the AMPAR phosphorylation ratio, which represents a readout of synaptic strength.

3.3.3 Induction of Synaptic Potentiation *in silico*

Inhibition from Purkinje cell takes essential roles in the regulation of sensory processing and plasticity in the vestibular system (Büttner et al. 1992; Ito et al. 1970). Here, I test whether hyperpolarisation can influence the synaptic strength, using the dual stimulation protocol used by McElvain et al. (2010) to produce LTP. Starting from 0 s, 550 ms of excitatory stimulation and 250 ms of hyperpolarisation to simulate strong inhibition from Purkinje cell are applied to all the electrical compartments for every 1 second. The Ca^{2+} dynamics in the middle compartment at one of the proximal dendrites (Figure R12B), which is characterised in Result 3.2.2, is used in the chemical model after converted to chemical Ca^{2+}. The relative AMPAR phosphorylation ratio shows a short (10 s) and small increase first, and then 30 s small decrease, and finally a progressive increase which reached 1.79 at 180 s. This result confirms that hyperpolarisation during excitatory stimulation can induce synaptic potentiation. Thus, together with the precious result, bidirectional plasticity in vestibular nerve synapse can be induced by different patterns of synaptic activity and hyperpolarisation caused by inhibitory stimulation from Purkinje cell can control the direction of this plasticity.

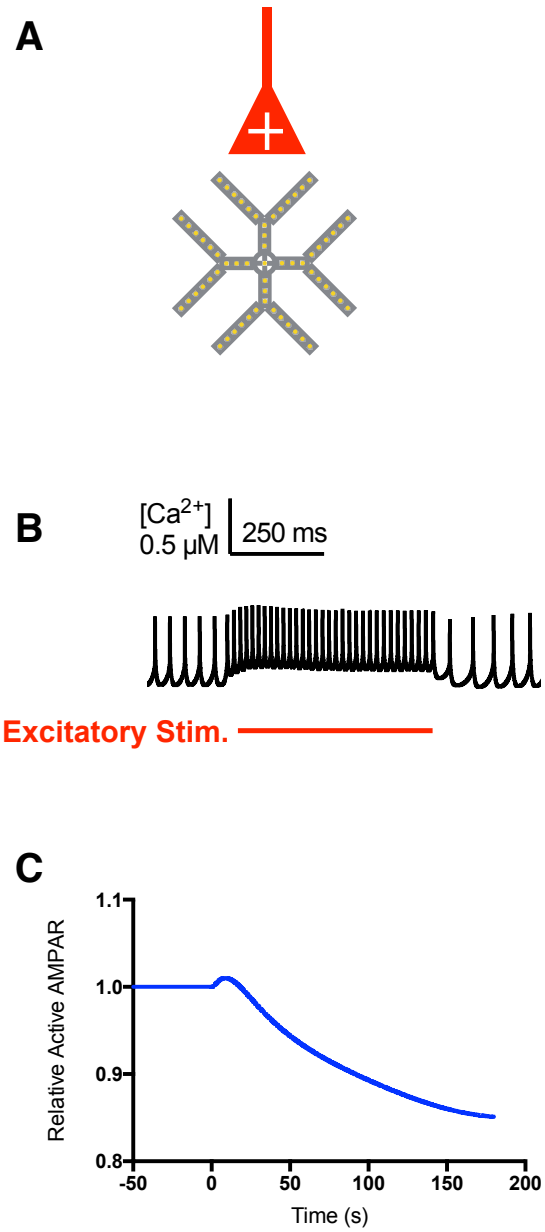

Figure R11. Induction of synaptic depression by excitatory stimulation only. (A) Schematic of single stimulation protocol, which comprises of 550 ms of 100 Hz vestibular nerve excitatory stimulation. (B) The [Ca^{2+}] dynamics in electrical model during excitatory stimulation. (C) The dynamics of relative AMPAR phosphorylation ratio when 1s dual stimulation protocol is applied starting at 0 s and is constantly repeated later. Synaptic depression is induced by this protocol.

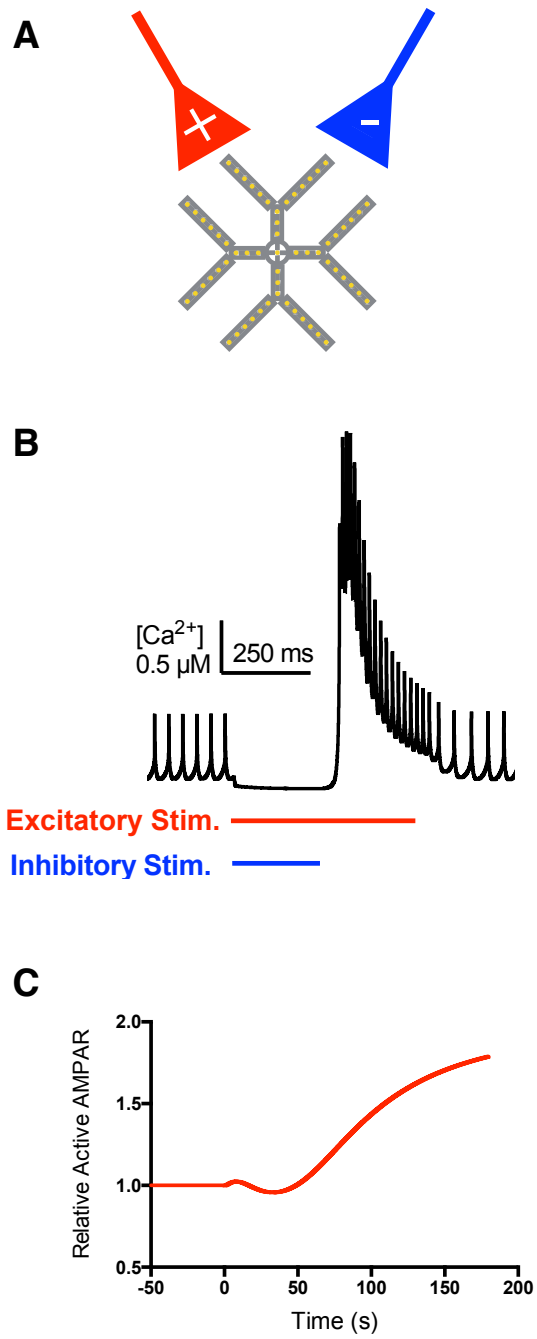

Figure R12. Induction of synaptic potentiation by paring excitatory stimulation with hyperpolarisation. (A) Schematic of dual stimulation protocol, which comprises 550 ms of 100 Hz vestibular nerve excitatory stimulation and 250 ms of hyperpolarisation to simulate strong inhibition from Purkinje cell. (B) The $[Ca^{2+}]$ dynamics in 1 s dual stimulation, where stimulation starts from 250 ms and ends in 800 ms. (C) The dynamics of relative AMPAR phosphorylation ratio when 1s dual stimulation protocol is applied in 0 s and constantly repeated. Synaptic potentiation is induced by this protocol.

3.3.4 Biochemical Mechanisms underlying Hyperpolarisation mediated Bidirectional Plasticity

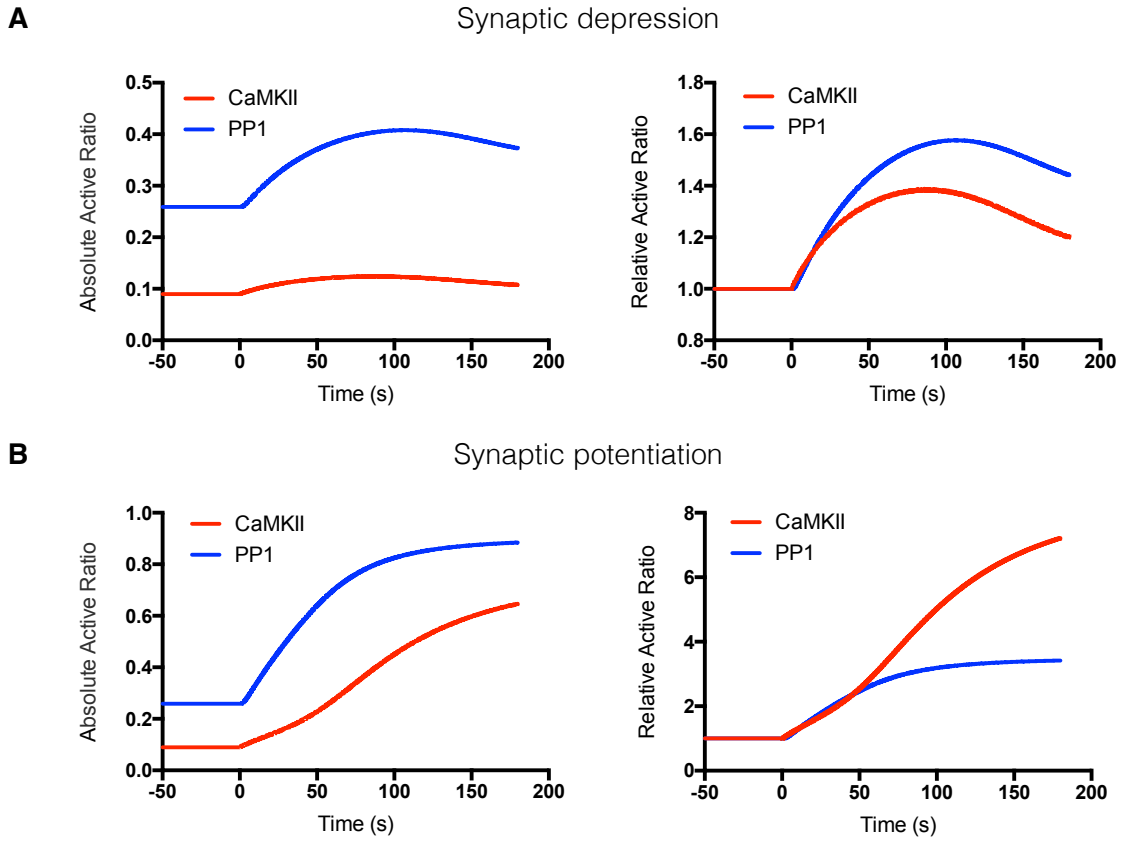

Figure R13. CaMKII and PP1 activation during bidirectional plasticity formation. The dynamics of absolute (left) and relative (right) active ratio of CaMKII and PP1 during synaptic depression (A) and potentiation (B).

The dynamics of AMPAR phosphorylation ratio in Figure R11 and R12C shares the same pattern of that in Figure R5. To further confirm that the biochemical mechanisms behind the bidirectional plasticity induced by my protocols are the same as that described in the biochemical result part (3.1.3), the dynamics of absolute and relative active ratio of CaMKII and PP1 during synaptic depression and potentiation are shown in Figure R13. In depression, a higher relative activation rate of CaMKII is observed at the beginning but for the rest time, the relative increase of PP2B is higher. In potentiation, a higher relative activation rate of CaMKII is observed at the beginning and then the relative increase of PP2B is higher later but after 50 s, the increase of active PP1 slows down and the continuous increase of CaMKII makes the relative active CaMKII higher than that of PP1. These also share the same pattern as the example shown in Figure R5.

4 Discussion

In this dissertation, I validated the complex biochemical model underlying bidirectional plasticity, explored the relationship between Ca^{2+} concentration and AMPAR phosphorylation ratio and analysed the kinetic mechanisms behind Ca^{2+}-dependent bidirectional plasticity. Then I implemented the stimulation protocols that induced vestibular synapse bidirectional plasticity in the electrical model of MVN B neuron, investigate the relationship between Ca^{2+} influx and different patterns of synaptic activity, and analysed the mechanisms underlying synaptic activity-dependent Ca^{2+} influx. Furthermore, I created a method to connect the electrical model in NEURON to a biochemical model in COPASI, and then simulated hyperpolarisation mediated bidirectional plasticity in my multi-scale model. My findings show that when MVN neuron receives excitatory stimulation from vestibular nerve, the moderate elevations of Ca^{2+} concentration that are mainly through NMDAR activation cause a higher increase degree of active PP1 (compared to active CaMKII), and consequently induce net dephosphorylation of AMPAR, resulting in synaptic depression. When the neuron receives excitatory stimulation from vestibular nerve combined with postsynaptic hyperpolarisation caused by Purkinje cell, the substantial elevations of Ca^{2+} concentration that are mainly through LVACC trigger the persistent autophosphorylation of CaMKII and the consequent higher increase degree of active CaMKII (compared to active PP1), inducing net phosphorylation of AMPAR and resulting in synaptic potentiation.

My findings provide a comprehensive understanding of the cellular and molecular mechanisms underlying hyperpolarisation mediated bidirectional plasticity in vestibular system and therefore contribute to a more mechanistic understanding of how the brain stores information and how I perfect our movement. In addition, the method I have created for multi-scale modelling allows linking any NEURON electrical model to a COPASI (and more general, SBML) biochemical model when they have common species.

Although the biochemical model used here is relatively complete, it does not include the late-phase changes in the system, such as AMPARs trafficking, transcription and translation of related components. In the future, models for AMPARs trafficking (Earnshaw & Bressloff 2006; Urakubo et al. 2008; Gallimore et al. 2016) and relevant protein synthesis (Aslam et al. 2009) should be added into my biochemical model to simulate the maintenance of LTP and LTD.

As for simulation method, spatial information is not included in my model but would be useful for simulating gene expression and membrane proteins activities. During this study, I tried MCELL(Stiles et al. 1996), a modelling tool for complex 3-D simulation of cellular micro-physiology. I created an MCELL version of my biochemical model. However, the model was very computationally intensive and would have taken a long time to simulate, even on the Eddie computing cluster available at the University of Edinburgh. This made it impractical for the time frame of the current project. A simplified biochemical model, an optimised simulation algorithm and/or a more advanced computer is required to do simulations on large spatial and temporal scales.

In this study, the protocols used by McElvain et al. (2010) were tested here and hyperpolarisation mediated bidirectional plasticity was confirmed only in proximal dendrites and only in MVN B neurons. I will carry on this project and perform simulations with different patterns of synaptic activity (e.g. the protocols used by Menzies et al 2010), and on distal dendrites and other types of neurons. I expect that the distal dendrites also show bidirectional plasticity that is gated by hyperpolarisation in MVN B neuron, and given the low density LVACC in other neurons like interneurons, synaptic potentiation may not be induced in other cells.

Regarding to the simulation tools, I uncovered a bug in COPASI version 4.16. It can produce wrong concentration readouts when dealing with a complex model with numerous events. Though the errors can be corrected manually, it does take time. Besides, the events function that I used to control the Ca^{2+} concentration, is not designed for this purpose. As a result, the speed of calculation is very slow (60 s in simulation per 24 h in real time). An accurate and fast version of COPASI is in a great demand. I have been in contact with the COPASI development team, who have informed me that the new version of COPASI currently under development has a new and more accurate mathematical system and that a function form inputting species concentrations from a file is under consideration. In addition to COPASI, I also tried MOOSE, the Multiscale Object-Oriented Simulation Environment (Dudani et al. 2014), which allows multi-scale stimulation of neural system ranging from subcellular components, biochemical reactions to complex models of single neurons, circuits, and large networks. Moose has a wide compatibility. It can interact with Matplotlib, PyQt, and OpenGL, and read kinetic models in GENESIS and SBML format and electrical models in NeuroML and Genesis format. However, I discovered that the chemical stimulator inside could not at the moment handle the SBML language correctly, and therefore I did not use it for my work. The MOOSE development team now is working on these issues. Once fixed, MOOSE may be a powerful and promising multi-scale stimulator

in neuroscience. Thus, a side effect of my work has been to uncover issues and inform the future development of two important biological simulation tools (COPASI and MOOSE), and has therefore been of service to the wider modelling and systems biology community.

References

Abarbanel, H.D.I., Huerta, R. & Rabinovich, M.I., 2002. Dynamical model of long-term synaptic plasticity. *Proceedings of the National Academy of Sciences of the United States of America*, 99(15), pp.10132–10137.

Albus, J.S., 1971. A theory of cerebellar function. *Mathematical Biosciences*, 10(1-2), pp.25–61.

Alkon, D.L. & Nelson, T.J., 1990. Specificity of molecular changes in neurons involved in memory storage. *The FASEB journal official publication of the Federation of American Societies for Experimental Biology*, 4(6), pp.1567–1576.

Angelaki, D.E., 2004. Eyes on target: what neurons must do for the vestibuloocular reflex during linear motion. *Journal of neurophysiology*, 92(1), pp.20–35.

Aslam, N. et al., 2009. Translational switch for long-term maintenance of synaptic plasticity. *Molecular systems biology*, 5(284), p.284. Available at: http://dx.doi.org/10.1038/msb.2009.38.

Aw, S.T. et al., 1996. Three-dimensional vector analysis of the human vestibuloocular reflex in response to high-acceleration head rotations. I. Responses in normal subjects. *Journal of neurophysiology*, 76(6), pp.4009–20. Available at: http://www.ncbi.nlm.nih.gov/pubmed/8985897\nhttp://www.ncbi.nlm.nih.gov/pubmed/8985896.

Bear, M.F. & Kirkwood, A., 1993. Neocortical long-term potentiation. *Current Opinion in Neurobiology*, 3(2), pp.197–202.

Bear, M.F. & Malenka, R.C., 1994. Synaptic plasticity: LTP and LTD. *Current Opinion in Neurobiology*, 4(3), pp.389–399.

Bhalla, U.S., 2002. Biochemical signaling networks decode temporal patterns of synaptic input. *Journal of Computational Neuroscience*, 13(1), pp.49–62.

Bhalla, U.S. & Iyengar, R., 1999. Emergent properties of networks of biological signaling pathways. *Science*, 283(5400), pp.381–387. Available at: papers2://publication/uuid/07895649-6152-4A9D-B6D1-1D65B4F39CE1\n0009888852\nhttp://www.sciencemag.org/content/283/5400/381.full.pdf.

Biber, A., Schmid, G. & Hempel, K., 1984. Calmodulin content in specific brain areas. *Experimental Brain Research*, 56(2), pp.323–326.

Bliss, T.V.P. & Lomo, T., 1973. Long-lasting potentiation of synaptic transmission in the dentate area of the anaesthetized rabbit following stimulation of the preforant path. *Journal of physiology*, 232, pp.331–356.

Boyden, E.S. et al., 2006. Selective Engagement of Plasticity Mechanisms for Motor

Memory Storage. *Neuron*, 51(6), pp.823–834.

Büttner, U., Straube, A. & Kurzan, R., 1992. Oculomotor effects of gamma-aminobutyric acid agonists and antagonists in the vestibular nuclei of the alert monkey. *Annals of the New York Academy of Sciences*, 656, pp.645–59. Available at: http://www.ncbi.nlm.nih.gov/pubmed/1599170 [Accessed July 27, 2016].

Calzone, L., Fages, F. & Soliman, S., 2006. BIOCHAM: An environment for modeling biological systems and formalizing experimental knowledge. In *Bioinformatics*. pp. 1805–1807.

Carnevale, N.T. & Hines, M.L., 2006. The NEURON Book. *Neuron*, 30(2), p.457. Available at: http://books.google.com/books?hl=en&lr=&id=YzcOyjKBPHgC&oi=fnd&pg=PA1&dq=The+Neuron+Book&ots=Ki6EKu_ZLd&sig=3Cd1R026GoIeT59HkXyV-xHm7Yo.

Carroll, R.C. et al., 1999. Rapid redistribution of glutamate receptors contributes to long-term depression in hippocampal cultures. *Nature neuroscience*, 2(5), pp.454–460.

Cimler, B.M. et al., 1985. P-57 is a neural specific calmodulin-binding protein. *Journal of Biological Chemistry*, 260(19), pp.10784–10788.

Citri, A. & Malenka, R.C., 2008. Synaptic plasticity: multiple forms, functions, and mechanisms. *Neuropsychopharmacology : official publication of the American College of Neuropsychopharmacology*, 33(1), pp.18–41. Available at: http://www.ncbi.nlm.nih.gov/pubmed/17728696.

Coomber, C., 1998. Current theories of neuronal information processing performed by Ca2+/calmodulin-dependent protein kinase II with support and insights from computer modelling and simulation. *Computers & chemistry*, 22, pp.251–263.

Crawford, J.D. & Vilis, T., 1991. Axes of eye rotation and Listing's law during rotations of the head. *Journal of neurophysiology*, 65(3), pp.407–423.

D'Alcantara, P., Schiffmann, S.N. & Swillens, S., 2003. Bidirectional synaptic plasticity as a consequence of interdependent Ca2+-controlled phosphorylation and dephosphorylation pathways. *European Journal of Neuroscience*, 17(12), pp.2521–2528.

Debanne, D., 1996. Associative synaptic plasticity in hippocampus and visual cortex: cellular mechanisms and functional implications. *Rev Neurosci*, 7(1), pp.29–46.

Dudani, N., Bhalla, U.S. & Ray, S., 2014. MOOSE, the Multiscale Object-Oriented Simulation Environment. In *Encyclopedia of Computational Neuroscience*. New York, NY: Springer New York, pp. 1–4. Available at: http://link.springer.com/10.1007/978-1-4614-7320-6_257-1 [Accessed July 28, 2016].

Earnshaw, B.A. & Bressloff, P.C., 2006. Biophysical model of AMPA receptor trafficking

and its regulation during long-term potentiation/long-term depression. *The Journal of neuroscience : the official journal of the Society for Neuroscience*, 26(47), pp.12362–73. Available at: http://www.jneurosci.org/content/26/47/12362.full [Accessed February 23, 2016].

ECCLES, J.C., 1964. *The Physiology of Synapses*, Available at: http://www.sciencedirect.com/science/article/pii/B9781483201030500223.

Franks, K.M., Bartol, T.M. & Sejnowski, T.J., 2001. An MCell model of calcium dynamics and frequency-dependence of calmodulin activation in dendritic spines. *Neurocomputing*, 38-40, pp.9–16. Available at: http://www.sciencedirect.com/science/article/pii/S0925231201004155 [Accessed February 22, 2016].

Frey, U. et al., 1988. Anisomycin, an inhibitor of protein synthesis, blocks late phases of LTP phenomena in the hippocampal CA1 region in vitro. *Brain Research*, 452(1-2), pp.57–65.

Fujita, M., 1982. Adaptive filter model of the cerebellum. *Biological Cybernetics*, 45(3), pp.195–206.

Funahashi, A. et al., 2003. CellDesigner: a process diagram editor for gene-regulatory and biochemical networks. *Biosilico*, 1(5), pp.159–162.

Gallimore, A.R. et al., 2016. A Computational Model for the AMPA Receptor Phosphorylation Master Switch Regulating Cerebellar Long-Term Depression. *PLOS Computational Biology*, 12(1), p.e1004664. Available at: http://dx.plos.org/10.1371/journal.pcbi.1004664 [Accessed January 29, 2016].

Gamble, E. & Koch, C., 1987. The dynamics of free calcium in dendritic spines in response to repetitive synaptic input. *Science (New York, N.Y.)*, 236(4806), pp.1311–5. Available at: http://www.ncbi.nlm.nih.gov/pubmed/3495885.

Graham, B.P., Menzies, J.R.W. & Dutia, M.B., 2009a. Model of hyperpolarization dependent LTD in MVN neurons. *BMC Neuroscience*, 10 (Supple, p.205.

Graham, B.P., Menzies, J.R.W. & Dutia, M.B., 2009b. Model of hyperpolarization dependent LTD in MVN neurons. *BMC Neuroscience*, 10 (Supple(4), p.205.

Hebb, D.O., 1949. *The Organization of Behavior*,

Hodgkin, A.L. & Huxley, A.F., 1952. A Quantitative Description of Membrane Current and its Application to Conduction and Excitation in Nerves. *J. Physiol.*, 117, pp.500–544.

Holmes, W.R. & Levy, W.B., 1990. Insights into associative long-term potentiation from computational models of NMDA receptor-mediated calcium influx and intracellular calcium concentration changes. *Journal of neurophysiology*, 63(5), pp.1148–1168.

Hoops, S. et al., 2006. COPASI - A COmplex PAthway SImulator. *Bioinformatics*, 22(24), pp.3067–3074.

Hughes, J.R., 1958. Post-tetanic potentiation. *Physiological reviews*, 38(1), pp.91–113.

Ito, M., 2002. Historical review of the significance of the cerebellum and the role of purkinje cells in motor learning. *Annals of the New York Academy of Sciences*, 978, pp.273–288.

Ito, M., Highstein, S.M. & Fukuda, J., 1970. *Cerebellar inhibition of the vestibulo-ocular reflex in rabbit and cat and its blockage by picrotoxin*,

Keller, R. et al., 2013. The systems biology simulation core algorithm. *BMC systems biology*, 7(1), p.55. Available at: http://www.pubmedcentral.nih.gov/articlerender.fcgi?artid=3707837&tool=pmcentrez&rendertype=abstract.

Klee, C.B., Ren, H. & Wang, X., 1998. Regulation of the calmodulin-stimulated protein phosphatase, calcineurin. *Journal of Biological Chemistry*, 273(22), pp.13367–13370.

Kotaleski, J.H. & Blackwell, K.T., 2010. Modelling the molecular mechanisms of synaptic plasticity using systems biology approaches. *Nature Reviews Neuroscience*, 11(4), pp.239–251. Available at: http://www.nature.com/doifinder/10.1038/nrn2807.

Kubota, Y. & Bower, J.M., 2001. Transient versus asymptomatic dynamics of CaM kinase II: Possible roles of phosphatase. *Journal of Computational Neuroscience*, 11(3), pp.263–279.

Li, L., Stefan, M.I. & Le Novère, N., 2012. Calcium Input Frequency, Duration and Amplitude Differentially Modulate the Relative Activation of Calcineurin and CaMKII. *PLoS ONE*, 7(9), p.e43810. Available at: http://dx.plos.org/10.1371/journal.pone.0043810.

Lisman, J., 1989. A mechanism for the Hebb and the anti-Hebb processes underlying learning and memory. *Proceedings of the National Academy of Sciences of the United States of America*, 86(23), pp.9574–9578.

Lledo, P.M. et al., 1995. Calcium/calmodulin-dependent kinase II and long-term potentiation enhance synaptic transmission by the same mechanism. *Proceedings of the National Academy of Sciences of the United States of America*, 92(24), pp.11175–9. Available at: http://www.pubmedcentral.nih.gov/articlerender.fcgi?artid=40594&tool=pmcentrez&rendertype=abstract.

Lledo, P.M. et al., 1998. Postsynaptic membrane fusion and long-term potentiation. *Science (New York, N.Y.)*, 279(5349), pp.399–403.

Lynch, G.S., Dunwiddie, T. & Gribkoff, V., 1977. Heterosynaptic depression: a postsynaptic correlate of long-term potentiation. *Nature*, 266(5604), pp.737–739.

Maletic-Savatic, M., Koothan, T. & Malinow, R., 1998. Calcium-evoked dendritic exocytosis in cultured hippocampal neurons. Part II: mediation by calcium/calmodulin-dependent protein kinase II. *The Journal of neuroscience : the official journal of the Society for*

Neuroscience, 18(17), pp.6814–6821.

Marr, D., 1969. A theory of cerebellar cortex. *The Journal of physiology*, 202(2), pp.437–470. Available at: http://www.pubmedcentral.nih.gov/articlerender.fcgi?artid=1351491&tool=pmcentrez&rendertype=abstract.

Mattioni, M. & Le Novère, N., 2013. Integration of biochemical and electrical signaling-multiscale model of the medium spiny neuron of the striatum. *PloS one*, 8(7), p.e66811. Available at: http://journals.plos.org/plosone/article?id=10.1371/journal.pone.0066811.

McElvain, L.E. et al., 2010. Bidirectional plasticity gated by hyperpolarization controls the gain of postsynaptic firing responses at central vestibular nerve synapses. *Neuron*, 68(4), pp.763–75. Available at: http://www.sciencedirect.com/science/article/pii/S0896627310007671.

McGlade-McCulloh, E. et al., 1993. Phosphorylation and regulation of glutamate receptors by calcium/calmodulin-dependent protein kinase II. *Nature*, 362(6421), pp.640–642. Available at: http://www.ncbi.nlm.nih.gov/entrez/query.fcgi?cmd=Retrieve&db=PubMed&dopt=Citation&list_uids=8385275.

Medina, J.F., 2010. A Recipe for Bidirectional Motor Learning: Using Inhibition to Cook Plasticity in the Vestibular Nuclei. *Neuron*, 68(4), pp.607–609. Available at: http://linkinghub.elsevier.com/retrieve/pii/S089662731000927X.

Menzies, J.R.W. et al., 2010. Synaptic plasticity in medial vestibular nucleus neurons: Comparison with computational requirements of VOR adaptation. *PLoS ONE*, 5(10), p.e13182. Available at: http://dx.plos.org/10.1371/journal.pone.0013182.

Michelson, S. & Schulman, H., 1994. CaM Kinase: A Model for its Activation and Dynamics. *Journal of Theoretical Biology*, 171(3), pp.281–290. Available at: http://www.sciencedirect.com/science/article/pii/S0022519384712318 [Accessed February 22, 2016].

Miles, F.A. & Lisberger, S.G., 1981. Plasticity in the vestibulo-ocular reflex: a new hypothesis. *Annual review of neuroscience*, 4, pp.273–99. Available at: http://www.ncbi.nlm.nih.gov/pubmed/6784658.

Morrison, A., Diesmann, M. & Gerstner, W., 2008. Phenomenological models of synaptic plasticity based on spike timing. *Biological Cybernetics*, 98(6), pp.459–478.

Mulkey, R.M. et al., 1994. Involvement of a calcineurin/inhibitor-1 phosphatase cascade in hippocampal long-term depression. *Nature*, 369(6480), pp.486–488. Available at: http://www.nature.com/nature/journal/v369/n6480/abs/369486a0.html.

Myers, C.J. et al., 2009. iBioSim: A tool for the analysis and design of genetic circuits.

Bioinformatics, 25(21), pp.2848–2849.

Naoki, H., Sakumura, Y. & Ishii, S., 2005. Local signaling with molecular diffusion as a decoder of Ca2+ signals in synaptic plasticity. *Molecular systems biology*, 1, p.2005.0027. Available at: http://www.pubmedcentral.nih.gov/articlerender.fcgi?artid=1681445&tool=pmcentrez&rendertype=abstract.

National Institute of Biomedical Imaging and Bioengineering, 2013. Computational Modeling. *Http://Www.Nibib.Nih.Gov/Science-Education/Science-Topics/Computational-Modeling*, (July).

Nguyen, P., Abel, T. & Kandel, E., 1994. Requirement of a critical period of transcription for induction of a late phase of LTP. *Science*, 265(5175), pp.1104–1107. Available at: http://science.sciencemag.org/content/265/5175/1104.abstract [Accessed February 23, 2016].

Le Novère, N., 2015. Quantitative and logic modelling of molecular and gene networks. *Nature reviews. Genetics*, 16(3), pp.146–58. Available at: http://www.ncbi.nlm.nih.gov/pubmed/25645874.

Le Novère, N. et al., 2009. The Systems Biology Graphical Notation. *Nature biotechnology*, 27(8), pp.735–741.

O'Connor, D.H., Wittenberg, G.M. & Wang, S.S.-H., 2005. Dissection of bidirectional synaptic plasticity into saturable unidirectional processes. *Journal of neurophysiology*, 94(2), pp.1565–73. Available at: http://www.ncbi.nlm.nih.gov/pubmed/15800079.

Pepke, S. et al., 2010. A dynamic model of interactions of Ca2+, calmodulin, and catalytic subunits of Ca2+/calmodulin-dependent protein kinase II. *PLoS Computational Biology*, 6(2).

Perkel, D.J. et al., 1993. The role of Ca2+ entry via synaptically activated NMDA receptors in the induction of long-term potentiation. *Neuron*, 11(5), pp.817–23. Available at: http://www.ncbi.nlm.nih.gov/pubmed/7902109.

Pfister, J.-P. & Gerstner, W., 2006. Triplets of spikes in a model of spike timing-dependent plasticity. *The Journal of neuroscience : the official journal of the Society for Neuroscience*, 26(38), pp.9673–9682. Available at: http://www.jneurosci.org/cgi/doi/10.1523/JNEUROSCI.1425-06.2006.

Pi, H.J. & Lisman, J.E., 2008. Coupled phosphatase and kinase switches produce the tristability required for long-term potentiation and long-term depression. *The Journal of neuroscience : the official journal of the Society for Neuroscience*, 28(49), pp.13132–8. Available at: http://www.pubmedcentral.nih.gov/articlerender.fcgi?artid=2620235&tool=pmcentrez&rendertype=abstract.

Porrill, J. & Dean, P., 2007. Cerebellar motor learning: When is cortical plasticity not enough? *PLoS Computational Biology*, 3(10), pp.1935–1950.

Quadroni, R. & Knöpfel, T., 1994. Compartmental models of type A and type B guinea pig medial vestibular neurons. *Journal of Neurophysiology*, 72(4), pp.1911–24. Available at: http://www.ncbi.nlm.nih.gov/pubmed/7529823.

Rall, W., 1959. Branching dendritic trees and motoneuron membrane resistivity. *Experimental Neurology*, 1(5), pp.491–527. Available at: http://www.sciencedirect.com/science/article/pii/0014488659900469.

Raymond, J.L. & Lisberger, S.G., 1998. Neural learning rules for the vestibulo-ocular reflex. *The Journal of neuroscience : the official journal of the Society for Neuroscience*, 18(21), pp.9112–9129.

van Rossum, M.C., Bi, G.Q. & Turrigiano, G.G., 2000. Stable Hebbian learning from spike timing-dependent plasticity. *The Journal of neuroscience : the official journal of the Society for Neuroscience*, 20(23), pp.8812–8821.

Rothman, J.S. et al., 2009. Synaptic depression enables neuronal gain control. *Nature*, 457(7232), pp.1015–1018. Available at: http://dx.doi.org/10.1038/nature07604.

Sabatini, B.L., Oertner, T.G. & Svoboda, K., 2002. The life cycle of Ca2+ ions in dendritic spines. *Neuron*, 33(3), pp.439–452. Available at: papers3://publication/uuid/AEAF4670-914B-4D71-B3ED-0AB4E4B8C8DF.

Saudargienė, A. & Graham, B.P., 2015. Inhibitory control of site-specific synaptic plasticity in a model CA1 pyramidal neuron. *Biosystems*, 130, pp.37–50. Available at: http://linkinghub.elsevier.com/retrieve/pii/S0303264715000349.

Schiegg, A. et al., 1995. Intracellular Ca2+ stores can account for the time course of LTP induction: a model of Ca2+ dynamics in dendritic spines. *J.Neurophysiol.*, 74(3), pp.1046–1055.

Shouval, H.Z., Bear, M.F. & Cooper, L.N., 2002. A unified model of NMDA receptor-dependent bidirectional synaptic plasticity. *Proceedings of the National Academy of Sciences*, 99(16), pp.10831–10836.

Song, S., Miller, K.D. & Abbott, L.F., 2000. Competitive Hebbian learning through spike-timing-dependent synaptic plasticity. *Nature neuroscience*, 3(9), pp.919–926.

Stefan, M.I., Edelstein, S.J. & Novere, N. Le, 2008. An allosteric model of calmodulin explains differential activation of PP2B and CaMKII. *Proceedings of the National Academy of Sciences*, 105(31), pp.10768–10773.

Stiles, J.R. et al., 1996. Miniature endplate current rise times less than 100 microseconds from improved dual recordings can be modeled with passive acetylcholine diffusion from a synaptic vesicle. *Proceedings of the National Academy of Sciences of the United States of America*, 93(12), pp.5747–5752.

Stone, L.S. & Lisberger, S.G., 1990. Visual responses of Purkinje cells in the cerebellar flocculus during smooth-pursuit eye movements in monkeys. II. Complex spikes. *Journal of neurophysiology*, 63(5), pp.1262–1275.

Takahashi, K. et al., 2004. A multi-algorithm, multi-timescale method for cell simulation. *Bioinformatics*, 20(4), pp.538–546.

Urakubo, H. et al., 2008. Requirement of an allosteric kinetics of NMDA receptors for spike timing-dependent plasticity. *The Journal of neuroscience : the official journal of the Society for Neuroscience*, 28(13), pp.3310–3323.

Zador, a, Koch, C. & Brown, T.H., 1990. Biophysical model of a Hebbian synapse. *Proceedings of the National Academy of Sciences of the United States of America*, 87(17), pp.6718–6722.

Zhabotinsky, A.M. et al., 2006. Role of the neurogranin concentrated in spines in the induction of long-term potentiation. *The Journal of neuroscience : the official journal of the Society for Neuroscience*, 26(28), pp.7337–7347.

Acknowledgements

Firstly, I would like to express my sincere gratitude to my supervisor Dr. Melanie Stefan for her supervision on the dissertation and input for my future career. You are a very nice person and good at education. And I would also like to thank my co-supervisor Prof. Mayank Dutia for the high frequency discussion and kind supervision on this project. At the same time, you are also a responsible program director and many thanks for all the organization and arrangement for our program. I really learnt a lot from you two supervisors.

In addition, I would like to thank Prof. Bruce Graham for kindly providing the scripts of electrical model as well as for the discussion on this project. To Prof. Nicolas Le Novere, thank you for the discussion on my project especially on SBGN, and for organising the *in silico* systems biology course. To Lu Li, thank you for providing the biochemical model as well as for the discussion about the biochemical model. Thank Prof. Sven Sahle for discussion on COPASI and thank Prof. Upinder S. Bhalla and Dr. Harsha Rani for discussion on MOOSE.

What's more, thank University of Edinburgh and Zhejiang University for providing this MSc program. And thank School of Medicine in ZJU for providing me scholarship.

Last but not least, I would like to thank my parents, my friends, the nice people in my office and the kind people in CIP for your company and support all the time.

Appendix

Table 1. Rate functions and parameters for the kinetics of active conductances

Channel and States Variable	Rate Functions		Minimal Value for τ_n (V)
	Activation	Inactivation	
g_{Na}	$g_{Na} = \bar{g}_{Na} *m^3*h^2$		
m	$\alpha_m = 5.0*exp(0.1*(V+39.5))$	$\beta_m = 5.0*exp(-0.044*(V+39.5))$	$\tau_{min} = 0.05$
h	$\alpha_h = 0.567*exp(-0.024*(V+35.0))$	$\beta_h = 0.567*exp(0.275*(V+35.0))$	$\tau_{min} = 0.3$
g_{Nap}	$g_{Nap} = \bar{g}_{Nap}*m$		$\tau_{min} = 1$
m	$\alpha_m = 0.12*exp(0.12*(V+56))$	$\beta_m = 0.12*exp(-0.03*(V+56))$	
g_H	$g_H = \bar{g}_H *n$		
n	$\alpha_n = 0.02/(1+exp((V+90)/7.5))$	$\beta_n = 0.02/(1+exp(-(V+90)/7.5))$	
$g_{bK\ (fast)}$	$g_{bK\ (fast)} = \bar{g}_{bK(fast)}*n^2$		$\tau_{min} = 0.8$
n	$\alpha_n = 5.82/(1+exp(-0.125*(V+3.3)))$	$\beta_n = 2.413/(1+exp(0.0675*(V+46.35)))$	
g_{AHP}	$g_{AHP} = \bar{g}_{AHP}*q^2$		
q	$\alpha_q = 3.5*10^9*[Ca2+]^3i$	$\beta_q = 0.074$	
$g_{K\ (slow)}$	$g_{K(slow)} = \bar{g}_{K(slow)}*n$		$\tau_{min} = 80.0$
n	$\alpha_n = 0.0015*exp(0.156*(V+45.0))$	$\beta_n = 0.0015*exp(-0.039*(V+45.0))$	
g_A	$g_A = \bar{g}_A*a^3*b$		
a	$\alpha_a = 0.2*exp(0.14*(V+65.0))$	$\beta_a = 0.2*exp(-0.035*(V+65.0))$	$\tau_{min} = 1.0$
b	$\alpha_b = 0.001*exp(-0.11*(V+71.0))$	$\beta_b = 0.01*exp(0.164*(V+71.0))$	$\tau_{min} = 24.0$
$g_{Ca(HVA)}$	$g_{Ca(HVA)} = \bar{g}_{Ca(HVA)}*s^2*r$		
s	$\alpha_s = 2.0/(1+exp(-(V+2)*0.054))$	$\beta_s = -0.08*(V+15.9)/(1-exp((V+15.9)*0.2))$	
r	$\alpha_r = min\ (0.01,\ 0.01*exp(-(V+60)/20))$	$\beta_r = 0.01 - \alpha r$	
$g_{Ca(LVA)}$	$g_{Ca(LVA)} = \bar{g}_{Ca(LVA)}*m^3*h$		
m	$\alpha_m = 3.3/(1.7+exp(-(V+28.8)/13.5))$		
	$\beta_m = 3.3*exp(-(V+63)/7.8/(1.7+exp(-(V+28.8)/13.5))$		
h	$\alpha_{1,2} = 2.5/(t*(1+k))$	$\beta_{1,2} = k*\alpha_{1,2}$	
	$\alpha_{2,3} = 2.5*exp(-(V+160.3)/17.8)$	$\beta_{2,3} = k*\alpha_{2,3}$	
	$k = (0.25+exp((V+83.5)/6.3)^1/2 - 0.5$	$t = 240/(1+exp(V+37.4)/30))$	

Table 2. Distribution and density of ionic conductances of MVN B neurons

Channels	Maximal Conductance per Membrane Area (μScm^{-2})		
	Soma	Proximal Dendrites	Distal Dendrite
$\bar{G}_{Na}$	43000	2880	0
$\bar{G}_{Nap}$	23.6	38	0
$\bar{G}_{H}$	66	66	0
$\bar{G}_{bK(fast)}$	37530	2572	640
$\bar{G}_{AHP}$	2716	0	0
$\bar{G}_{K(slow)}$	519	406	0
$\bar{G}_{A}$	755	0	0
$\bar{G}_{Ca(HVA)}$	2385	1417	350
$\bar{G}_{Ca(LVA)}$	166	651/1607	50
$\bar{G}_{Na(leak)}$	37.8	0.7	0.71
$\bar{G}_{Ca(leak)}$	74.6	1	1
$\bar{G}_{K(leak)}$	166	3.69	3.68

Table 3. Initial Concentration of molecular species

Name	Concentration M
CamR	1.45E-09
CamT	10.00E-05
CaMKII	7.00E-05
PP2Bi	6.00E-06
Darpp-32	3.00E-06
PKA	1.20E-08
PP1a	2.00E-06
AMPAR_P	1.66E-07
AMPAR	1.49E-06

Supplementary information

Dropbox link:

https://www.dropbox.com/sh/qnz53kb2skz986b/AADYRyb1iSnTZB89hPY_DzYTa?dl=0

List of Files:

1. Biochemical model in COPASI format (BiochemicalModel.cps).
2. Biochemical model in SBML format (BiochemicalModel.xml).
3. Parameters description Biochemical model (BiochemicalParameters folder)
4. Electrical model in NEURON format (Neuron folder)